eventually achieve appreciable transfection efficiency even for systems without high endosomal-disrupting properties, including PLys-based polyplex systems.

Experimental Section

Materials. *N*,*N*-Diisopropylethylamine (DIEA), dithiothreitol (DTT), aphidicolin, and D-luciferin were purchased from Wako Pure Chemical Industries (Osaka, Japan). *N*-Methyl-2-pyrrolidone (NMP) was purchased from Aldrich Chemical (Milwaukee, WI). *N*-Succinimidyl 3-(2-pyridyldithio)-propionate (SPDP) was purchased from Dojindo Laboratories (Kumamoto, Japan). Cyclo[RGDfK(CX-)] (c(RGDfK)) peptides (X = 6-aminocaproic acid: ε-Acp) was purchased from Peptide Institute (Osaka, Japan). Acetal-poly(ethylene glycol)-*block*-poly(lysine) (acetal-PEG-PLys) and c(RGDfK)-PEG-PLys block copolymers (PEG, 12 000 g/mol; polymerization degree of PLys segment, 72; introduction rate of c(RGDfK) peptide, 66%) were synthesized as previously reported.[11] A micro-BCA protein assay reagent kit was purchased from Pierce Chemical (Rockford, IL). The luciferase assay kit was a product of Promega (Madison, WI). Plasmid pCAcc+Luc coding for firefly luciferase under the control of the CAG promoter was provided by RIKEN Gene Bank (Tsukuba, Japan), amplified in competent DH5α *Escherichia coli*, and then purified using a HiSpeed Plasmid MaxiKit purchased from Qiagen Sciences (Germantown, MD).

Synthesis of Block Copolymers: (a) Acetal-poly(ethylene glycol)-block-poly[ε-3-(2-pyridyldithio)propionyl lysine] (Acetal-PEG-P(Lys-PDP)). Pyridyldithiopropionyl (PDP) groups were introduced to the PLys side chain by the use of a heterobifunctional reagent, SPDP. The typical synthesis procedure is described as follows for the acetal-PEG-P(Lys-PDP) (5 mol % PDP): Acetal-PEG-PLys (200 mg, 8.38 μmol) and SPDP (11.7 mg, 37.7 μmol) were separately dissolved in NMP containing 5 wt % LiCl (10 mL for acetal-PEG-PLys, 1 mL for SPDP). A solution containing SPDP and DIEA (1.05 mL, 377 μmol) was added to acetal-PEG-PLys solution and stirred at room temperature for 3 h. The mixture was then precipitated into an approximately 20-times-excess volume of diethyl ether. The polymer was dissolved in 10 mM phosphate buffer (pH 7.0) with 150 mM NaCl, dialyzed against the same buffer solution and distilled water, and lyophilized to obtain acetal-PEG-P(Lys-PDP) (166 mg, 80%).

(b) c(RGDfK)-poly(ethylene glycol)-block-poly[ε-(3-mercaptopropinonyl) lysine] (c(RGDfK)-PEG-P(Lys-MP)). The typical synthesis procedure is described as follows for the c(RGDfK)-PEG-P(Lys-MP) (5 mol % MP): Acetal-PEG-P(Lys-PDP) (30 mg, 1.21 μmol) was dissolved in 10 mM Tris-HCl buffer solution (pH 7.4) (3 mL) with DTT (6.76 mg, 43.9 μmol). After 30 min incubation at room temperature, the polymer solution was dialyzed against 0.2 M AcOH buffer (pH 4.0). c[RGDfK(CX-)] (10.4 mg, 12.8 mmol) in AcOH buffer (3 mL) was then added to the polymer solution. After stirring for 5 days, DTT (6.67 mg, 43.9 μmol) was added and stirred at room temperature for 3 h. The reacted polymer was purified by dialysis sequentially against 10 mM phosphate buffer (pH 7.0) with 150 mM NaCl and distilled water, and lyophilized to obtain c(RGDfK)-PEG-P(Lys-MP) (20.5 mg, 71%).

The ^{1}H NMR spectrum of each polymer was obtained with an EX300 spectrometer (JEOL, Tokyo, Japan). Chemical shifts were reported in ppm relative to the residual protonated solvent resonance. Block copolymer with X% of thiolation degree was abbreviated as B-SHX%.

Preparation of Polyplex Micelles. Each thiolated block copolymer was dissolved in 10 mM Tris-HCl buffer (pH 7.4), followed by the addition of 3-times-excess mol of DTT against the PDP or MP group. After 30 min incubation at room temperature, the polymer solution in varying concentrations was added to a twice-excess volume of 50 μg/mL pDNA/10 mM Tris-HCl (pH 7.4) solution to form polyplex micelles with different compositions. The final pDNA concentration was adjusted to 33.3 μg/mL. The N/P ratio was defined as the residual molar ratio of amino groups of PLys to the phosphate groups of pDNA. After overnight incubation at room temperature, the polyplex micelle solution was dialyzed against 10 mM Tris-HCl (pH 7.4) containing 0.5 vol% DMSO at 37 °C for 24 h to remove the impurities, followed by 2 days of additional dialysis to remove DMSO. During the dialysis, the thiol groups of thiolated block copolymers were oxidized to form disulfide cross-links. To follow the oxidation process, the remaining thiol groups in disulfide cross-linked micelles were determined by Ellmah's method.[15] Polyplex micelles with and without cyclic RGD peptide ligands were abbreviated as RGD (+) and RGD (−) micelles, respectively.

Dynamic Light Scattering Measurement. The sizes of the polyplex micelles were evaluated by dynamic light scattering (DLS) using the Nano ZS zetasizer (ZEN3600, Malvern Instruments, Worcestershire, U.K.). A He−Ne ion laser (633 nm) was used for the incident beam. Polyplex micelle solutions (33.3 μg pDNA/mL) with an N/P = 2 in 10 mM Tris-HCl (pH 7.4) were used for the measurements. The data obtained at a detection angle of 173 ° and a temperature of 25 °C were analyzed by a cumulant method to obtain the hydrodynamic diameters and polydispersity indices (μ/Γ^2) of the micelles. The results reported were expressed as mean values (± SEM) of four experiments.

ζ-Potential Measurement. The ζ-potentials of the polyplex micelles were evaluated by the laser-doppler electrophoresis method using Nano ZS with a He−Ne ion laser (633 nm). Polyplex micelle solution with an N/P = 2 was adjusted to a concentration of 20 μg pDNA/mL. The ζ-potential was measured at 25 °C. A scattering angle of 173 ° was used in these measurements. The results were expressed as the mean values (± SEM) of four experiments.

Atomic Force Microscopy (AFM) Imaging. Five microliters of each sample was deposited on a freshly cleaved

(15) Riddles, P. W.; Blakeley, R. L.; Zerner, B. Ellman's Reagent: 5,5′-Dithiobis(2-nitrobenzoic Acid)- a Reexamination. *Anal. Biochem.* **1979**, *94*, 75–81.

Scheme 1. Synthesis Route of c(RGDfK)-PEG-P(Lys-MP) Block Copolymer

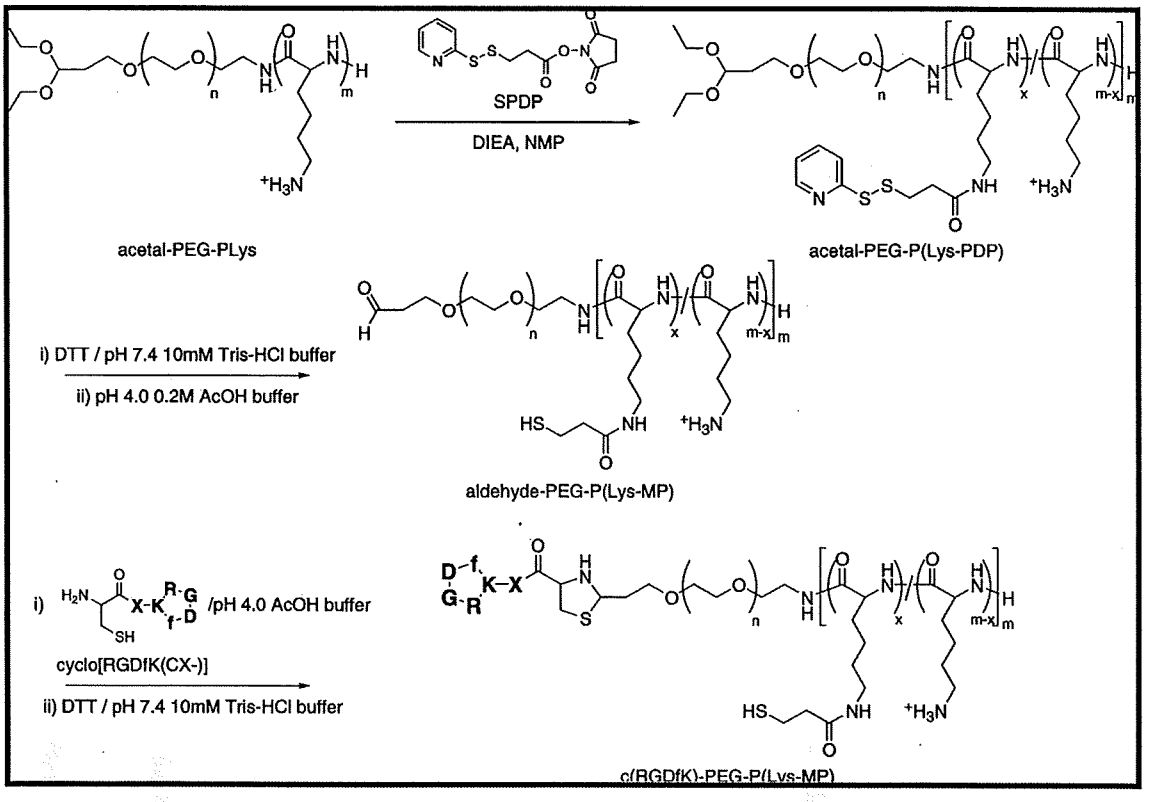

mica substrate for 30 s and then adequately dried under a gentle flow of nitrogen gas. AFM imaging was performed in a tapping mode with MPP-11100 (Vecco Instruments, Woodbury, NY) on a Nano Scope (Vecco Instruments) operated by Nanoscope IIIa software (Digital Instruments, Santa Barbara, CA). The cantilever oscillation frequency was

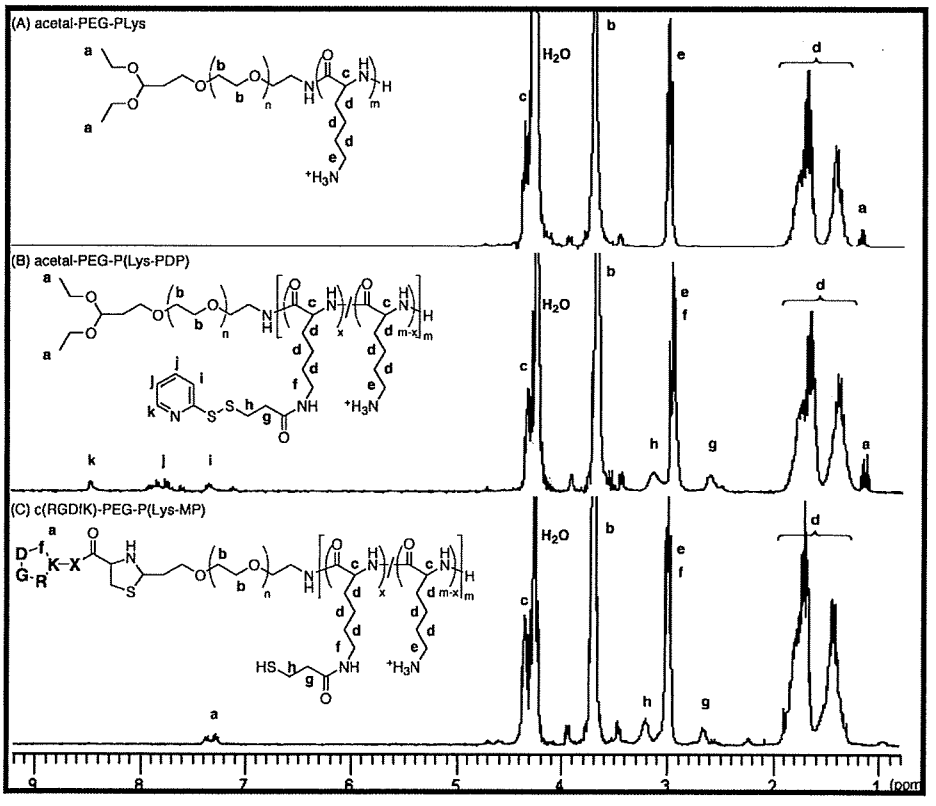

Figure 1. ^{1}H NMR spectra of acetal-PEG-PLys (A), acetal-PEG-P(Lys-PDP) (B-SH5%) (B), and c(RGDfK)-PEG-P-(Lys-MP) (B-SH5%) (C) in D_2O at 80 °C.

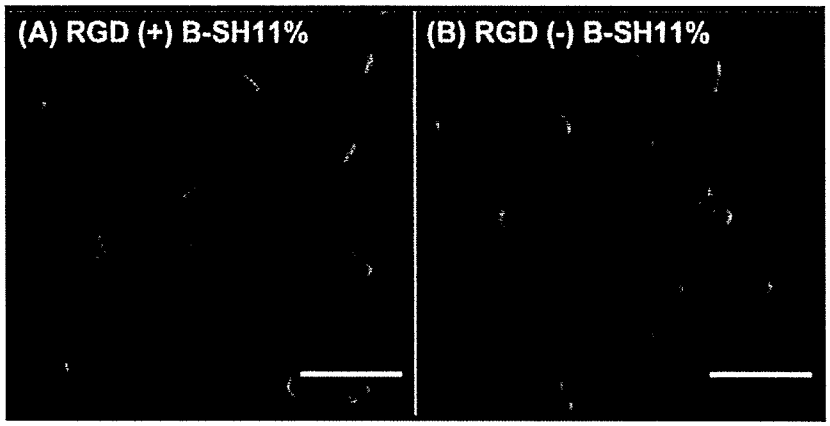

Figure 2. AFM images of cross-linked micelles (B-SH11%, N/P = 2) with (A) or without (B) cyclic RGD peptide ligands. The scale bars represent 500 nm.

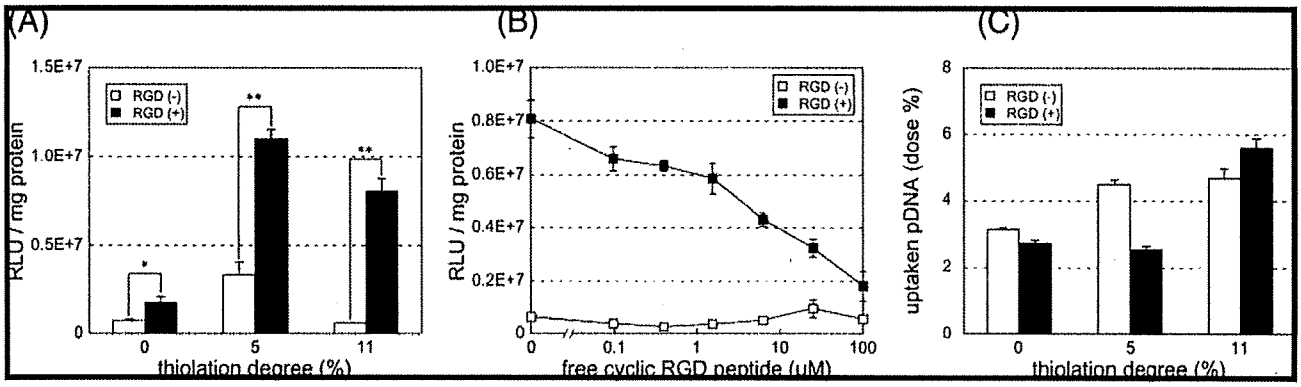

Figure 3. In vitro transfection efficiency and cellular uptake of polyplex micelles against HeLa cells. (A) Effects of cyclic RGD peptide ligands on transfection efficiency for micelles with varying thiolation degrees (N/P = 2). (B) Inhibitory effect of free cyclic RGD peptide on the transfection with B-SH11% polyplex micelles (N/P = 2) with or without cyclic RGD peptide ligands. (C) Cellular uptake of RGD (+) and RGD (−) polyplex micelles (N/P = 2) loading ^{32}P-labeled pDNA. Error bars in the graphs represent SEM, $n = 4$. $P^* < 0.05$ and $P^{**} < 0.01$.

tuned to the resonance frequency of the cantilever, 260−340 kHz. The images were recorded at a 2 μm/s linear scanning speed and with a sampling density of 61 nm^2 per pixel. Raw AFM images were processed only by background removal (flattening) using a microscope manufacturer's image-processing software.

Transfection. HeLa cells were seeded on 24-well culture plates (10 000 cells/well) and incubated overnight in 500 μL of Dulbecco's modified Eagle's medium (DMEM) containing 10% fetal bovine serum (FBS). The medium was replaced with fresh medium, after which polyplex solution (N/P = 2) was applied to each well (1 μg of pDNA/well). After 24 h incubation, the medium was replaced with 500 μL of fresh medium, followed by 24 h reincubation. The luciferase gene expression was then evaluated based on the intensity of photoluminescence intensity using the Luciferase assay kit and a Lumat LB9507 luminometer (Berthold Technologies, Bad Wildbad, Germany). The amount of protein in each well was concomitantly determined using a Micro BCA protein assay reagent kit.

Inhibitory Effect of Free Cyclic RGD Peptides. HeLa cells were seeded on 24-well culture plates (10 000 cells/well) and incubated overnight in 500 μL of DMEM containing 10% FBS. The medium was replaced with fresh medium containing various concentrations of cyclo[RGDfK(CX-)], followed by 3 h incubation. The polyplex micelle solution (B-SH11%, N/P = 2) was applied to each well (1 μg pDNA/well). After 24 h incubation, the medium was replaced with 500 μL of fresh medium, followed by 24 h reincubation. The luciferase gene expression was then evaluated in the same way as described in the Transfection section.

Analysis of Cellular Uptake of Polyplex Micelles. pDNA was radioactively labeled by incorporation of ^{32}P-dCTP (GE Healthcare U.K., Buckinghamshire, U.K.) using a nick translation system (Invitrogen, Carlsbad, CA) according to the manufacturer's protocol. Unincorporated nucleotides were carefully removed using the High Pure PCR Product Purification Kit (Roche, Basel, Switzerland). HeLa cells were seeded on 24-well culture plates (10 000 cells/well) and incubated overnight in 500 μL of DMEM containing 10% FBS. The medium was replaced with fresh medium, after which the polyplex micelle incorporating the mixture of nonlabeled and ^{32}P-labeled pDNA (N/P = 2) was applied to each well (1 μg pDNA/well). After 24 h incubation, the medium was removed and the cells were washed 3 times with PBS. The cells were lysed with 400 μL of cell culture lysis reagent (Promega) for 30 min at room temperature, after which the lysate was mixed with 5 mL of Ultima Gold

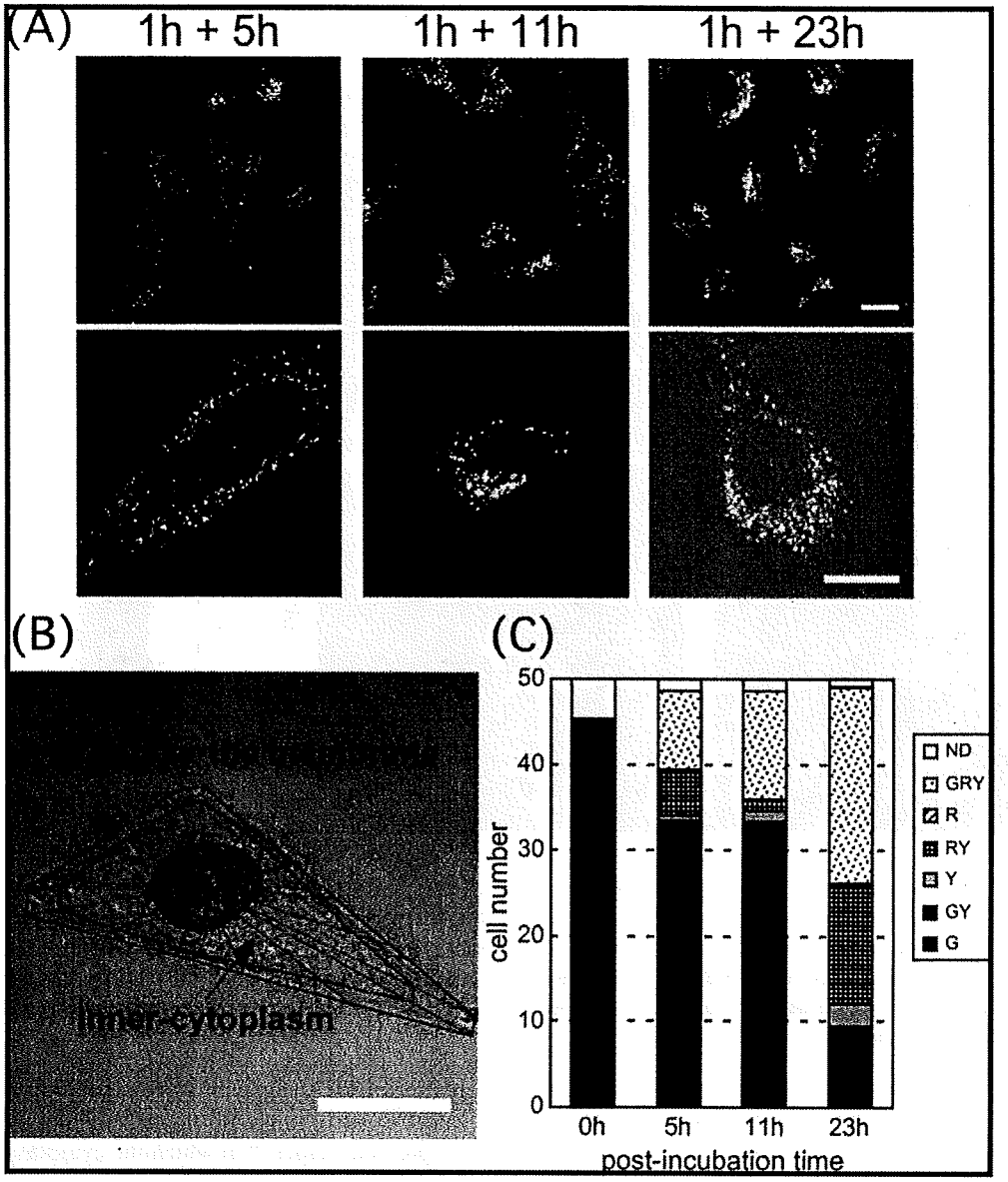

Figure 4. Intracellular distribution B-SH11% polyplex micelles (N/P = 2). RGD (−) micelles loading Cy5-labeled pDNA (red) and RGD (+) micelles loading Cy3-labeled pDNA (green) were simultaneously added and incubated with HeLa cells for 1 h. After replacement with fresh medium, cells were reincubated for the indicated reincubation times (5 h, 11 h, 23 h). (A) CLSM images. Scale bars represent 20 μm. (B) Definitions of "nucleus", "inner-cytoplasm", and "in or near the membrane" regions. "Inner-cytoplasm" was defined as three-quarters of the area from the nucleus to the cell membrane, and "in or near the membrane" was defined as the remaining quarter on the side of the cell membrane. (C) Quantitative analysis of the inner-cytoplasmic distribution of pDNA transfected by polyplex micelles with or without RGD ligands. Fifty different cells were observed and evaluated for each time point. G: green (Cy3-labeled pDNA loaded in RGD (+) micelles). R: red (Cy5-labeled pDNA loaded in RGD (−) micelles). Y: yellow (colocalized Cy3-labeled and Cy5-labeled pDNAs). ND: not detectable (no colors detectable from pDNA).

(Perkin-Elmer, Waltham, MA). Measurements were performed using the Tricarb 2200CA liquid scintillation analyzer (Packard, Meriden, CT) with a counting time of 1 min. The amounts of uptaken pDNA were calculated using a standard curve calibrated with naked ^{32}P-labeled pDNA.

CLSM Observation. pDNA was labeled with Cy3 or Cy5 according to the manufacturer's protocol. Briefly, pDNA was labeled using the Label IT Nucleic Acid Labeling Kit (Mirus, Madison, WI). HeLa cells (30 000 cells) were seeded on a 35 mm glass base dish (Iwaki, Tokyo, Japan) and incubated overnight in 1 mL of DMEM containing 10% FBS, followed by replacement with fresh medium. In the simultaneous observation of RGD (−) and RGD (+) micelles (Figure 4), RGD (−) B-SH11% polyplex micelle solution containing 3 μg Cy5-labeled pDNA (N/P = 2) and RGD (+) B-SH11% polyplex micelle solution containing 3 μg Cy3-labeled pDNA (N/P = 2) were simultaneously applied to a glass dish with cultured HeLa cells. The measurement condition was adjusted so as to obtain almost the same fluorescence intensities between RGD (+) B-SH11% micelles containing Cy3-

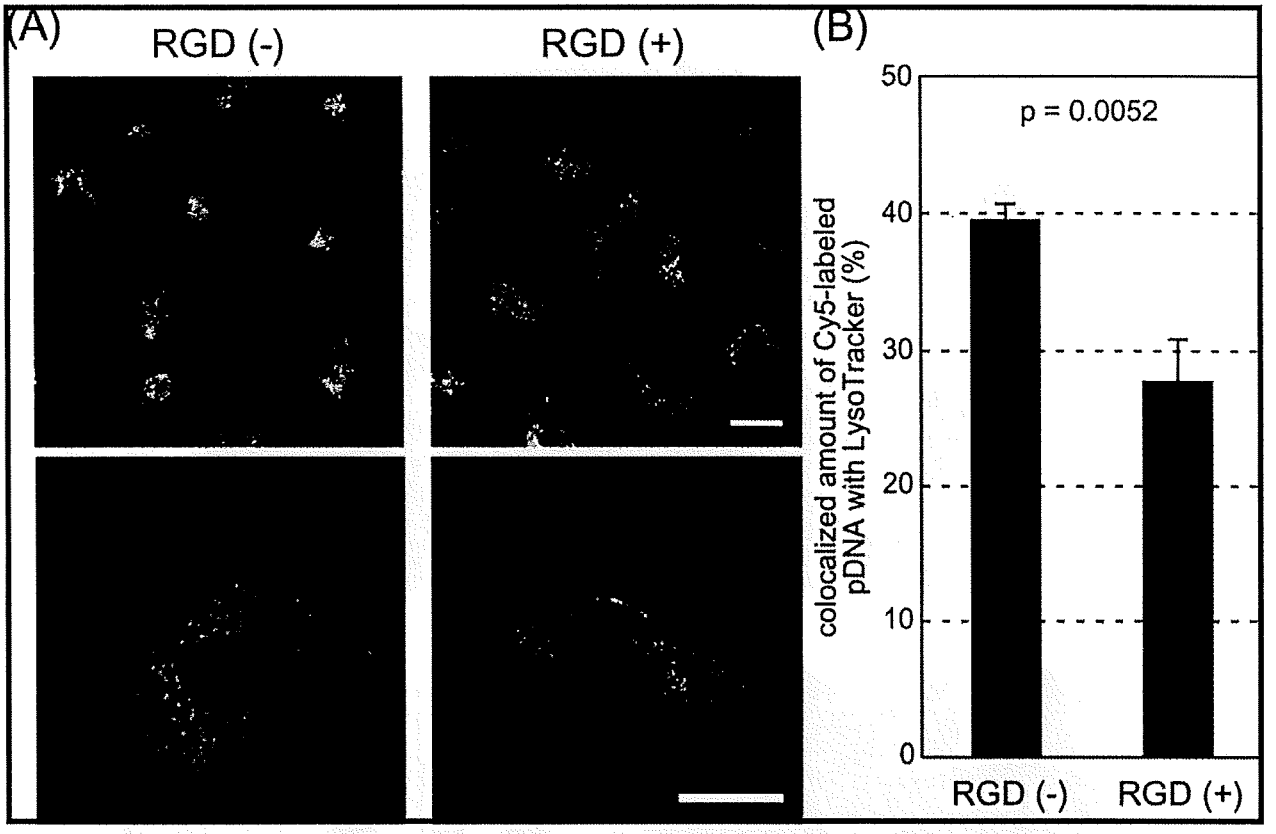

Figure 5. Distribution of RGD (+) and RGD (−) B-SH11% polyplex micelles (N/P = 2) in late endosomes and lysosomes. Polyplex micelles loading Cy5-labeled pDNA (red) were incubated with HeLa cells for 1 h. After replacement with fresh medium, the cells were reincubated for 11 h. The cell nuclei were stained with Hoechst 33342 (blue), and the acidic late endosomes and lysosomes were stained with LysoTracker Green (green). (A) CLSM images of the cells transfected with RGD (−) micelles (left) and RGD (+) micelles (right). The scale bars represent 20 μm. (B) Quantification of Cy5-labeled pDNA colocalized with LysoTracker Green in the inner-cytoplasm. Error bars in the graph represent SEM (n = 10).

labeled pDNA and RGD (+) B-SH11% micelles containing Cy5-labeled pDNA. In the observation with organelle staining (Figures 5 and 6), either RGD (−) or RGD (+) B-SH11% polyplex micelle solution containing Cy5-labeled pDNA (N/P = 2) was applied to a dish with cultured HeLa cells. After various incubation periods, the medium was removed and the cells were washed 3 times with PBS. The intracellular distribution of the polyplex micelles was observed by CLSM after staining acidic late endosomes and lysosomes with LysoTracker Green (Molecular Probes, Eugene, OR), lipid rafts and caveosomes with cholera toxin subunit B (CT-B) Alexa Fluor 488 conjugate (Molecular Probes), and the nuclei with Hoechst 33342 (Dojindo Laboratories, Kumamoto, Japan). The CLSM observation was performed using an LSM 510 (Carl Zeiss, Oberlochen, Germany) with a C-Apochromat 63X objective (Carl Zeiss) at the excitation wavelength of 488 nm (Ar laser) for LysoTracker Green and CT-B Alexa Fluor 488, 543 nm (He−Ne laser) for Cy3, 633 nm (He−Ne laser) for Cy5, and 710 nm (MaiTai laser, two photon excitation; Spectra-Physics, Mountain View, CA) for Hoechst 33342, respectively.

Evaluation of Intracellular Distribution of Polyplex Micelles. To evaluate the amounts of polyplex micelles in cytoplasm, polyplex micelles internalized into the inner region of the cytoplasm were distinguished from polyplex micelles adsorbing onto the cell membrane by reference to a previous paper,[16] in which the cytoplasm was divided into four quadrants to study the intracellular spatial variation of polyplexes (Figure 4B). First, an intracellular region was divided into three areas: "nucleus", "inner-cytoplasm", and "in or near the membrane". "Inner-cytoplasm" was defined as a three-quarters of the area from the nucleus to the cell membrane, and "in or near the membrane" was defined as remaining quarter area on the side of the cell membrane, as illustrated in Figure 4B. From the observation of 50 different cells, the relative amounts of RGD (−) micelles (red) and RGD (+) micelles (green) in the "inner-cytoplasm" were determined based on the number of cells. The following abbreviations are used in Figure 4C: G, green (Cy3-labeled pDNA); R, red (Cy5-labeled pDNA); Y, yellow (Cy3-labeled pDNA colocalized with Cy5-labeled pDNA); and ND, not detectable (no colors (pDNA) detectable). In brief, GRY represents cells with green, red, and yellow spots indepen-

(16) Suh, J.; Wirts, D.; Hanes, J. Efficient Active Transport of Gene Nanocarriers to the Cell Nucleus. *Proc. Natl. Acad. Sci. U.S.A.* **2003**, *100*, 3878–3882.

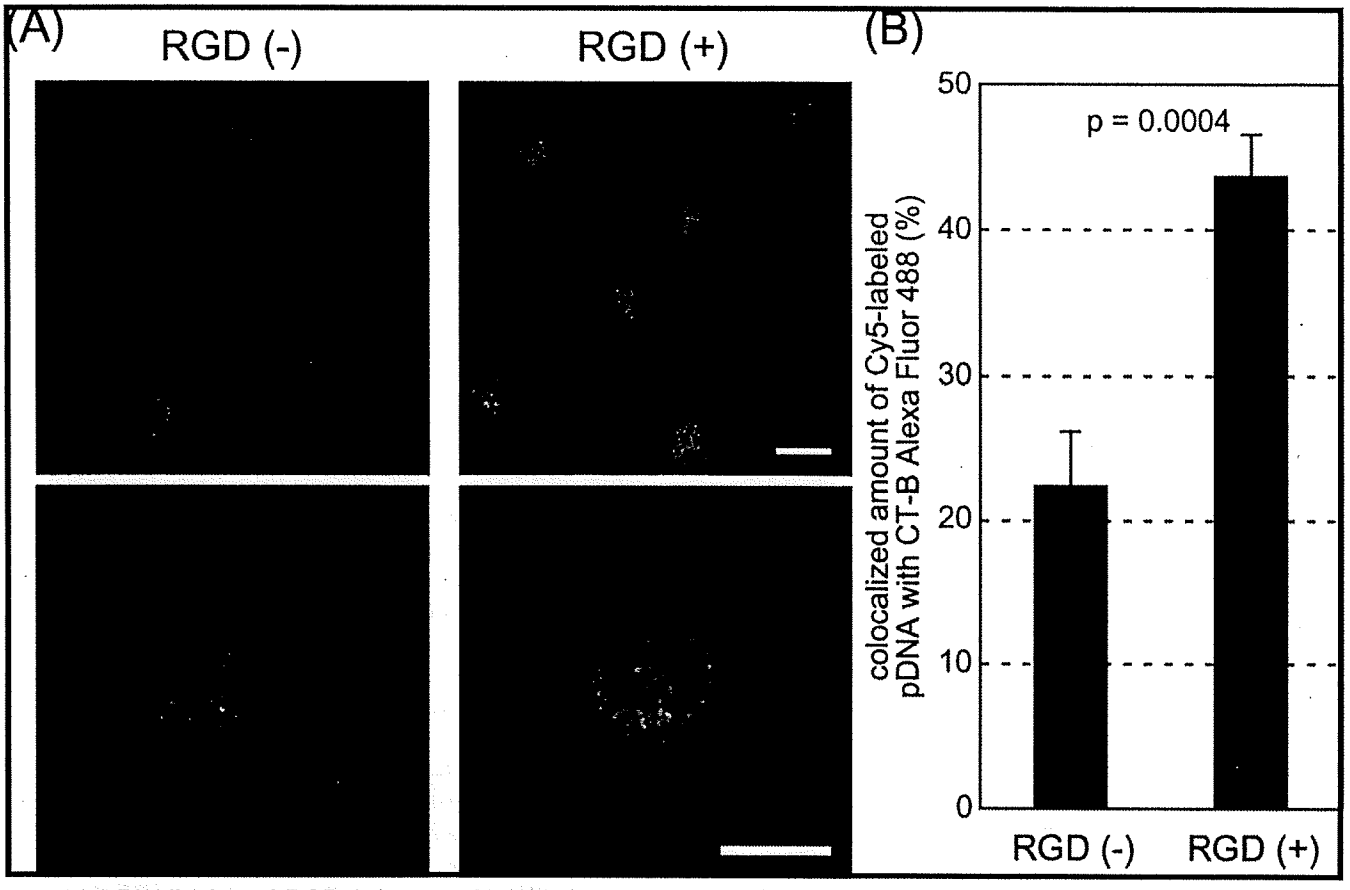

Figure 6. Distribution of RGD (+) and RGD (−) B-SH11% polyplex micelles (N/P = 2) in lipid rafts and caveosomes. Polyplex micelles loading Cy5-labeled pDNA (red) and CT-B Alexa Fluor 488 conjugate (green) were incubated with HeLa cells for 1 h. After replacement with fresh medium, the cells were reincubated for 11 h. The cell nuclei were stained with Hoechst 33342 (blue). (A) CLSM images of RGD (−) micelles (left) and RGD (+) micelles (right). The scale bars represent 20 μm. (B) Quantification of Cy5-labeled pDNA colocalized with CT-B in the inner-cytoplasm. Error bars in the graph represent SEM (n = 10).

dently existing in the "inner-cytoplasm", and GY represents cells with green and yellow spots but without red spots.

To evaluate the final destinations of polyplex micelles, the rate of colocalization of Cy5-labeled pDNA with LysoTracker Green or CT-B Alexa Fluor 488 was quantified (Figures 5B and 6B). LysoTracker Green was used as a marker for the late endosomes and the lysosomes, and CT-B Alexa Fluor 488 was used as a marker for the lipid rafts and the caveosomes. Colocalization was quantified as follows:

$$\text{amount of colocalization (\%)} = \text{Cy5 pixels}_{\text{colocalization}}/\text{Cy5 pixels}_{\text{total}} \times 100$$

where Cy5 $\text{pixels}_{\text{colocalization}}$ represents the number of Cy5 pixels colocalizing with LysoTracker Green or CT-B Alexa Fluor 488 in the inner-cytoplasm, and Cy5 $\text{pixels}_{\text{total}}$ represents the number of all Cy5 pixels in the inner-cytoplasm.

Real-Time Luciferase Gene Expression. HeLa cells (40 000 cells) were seeded on a 35 mm dish (Becton Dickinson, Franklin Lakes, NJ) and incubated overnight in 2 mL of DMEM containing 10% FBS, with or without 10 μg/mL aphidicolin for synchronization of cells. The HeLa cell cycle was arrested in a phase between G1 and S by over 16 h incubation with aphidicolin.[17] The subsequent replacement with fresh medium let cells start to divide at 13 h later. In this assay, three experimental conditions were used to regulate the lag between the time the polyplex micelles were added and the beginning of mitosis. First was the "normal" condition, meaning without any treatments for synchronization. Second was the "3 h mitosis" condition, where each polyplex micelle was added 10 h after the replacement of medium containing aphidicolin with fresh medium, thus setting the start of cell mitosis 3 h after the addition of polyplex micelles. Third was the "13 h mitosis" condition, where each polyplex micelle was added just after the medium replacement, thus commencing cell mitosis 13 h after the addition of the micelles. In the case of the "normal" and "13 h mitosis" conditions, after replacement with fresh medium containing 0.1 mM D-luciferin, RGD (−) or RGD (+) B-SH11% polyplex micelles (N/P = 2) containing 3 μg of pDNA were immediately added. In the case of the "3 h

(17) Pedrali-Noy, G.; Spadari, S.; Miller-Faures, A.; Miller, A. O. A.; Kruppa, J.; Koch, G. Synchronization of HeLa Cell Cultures by Inhibition of DNA Polymerase α with Aphidicolin. *Nucleic Acids Res.* **1980**, *8*, 377–387.

mitosis" condition, polyplex micelles were added 10 h after the replacement with fresh medium containing 0.1 mM D-luciferin. The dishes were set in a luminometer incorporated in a CO_2 incubator (AB-2550 Kronos Dio, ATTO, Tokyo, Japan), and the bioluminescence was monitored every 20 min with an exposure time of 2 min.

Results

Synthesis of c(RGDfK)-PEG-P(Lys-MP). (Scheme 1). Thiolation of acetal-PEG-PLys block copolymer was carried out using a previously described method.[9] Briefly, SPDP was used as a thiolating reagent and reacted with ε-amino group of Lys unit; consequently, a 3-(2-pyridyldithio)propionyl (PDP) group was introduced via an amide bond. Note that the introduction of the thiol group by SPDP decreased the cationic charge density of the PLys segment as the introduction rate increased. Thiolated acetal-PEG-P(Lys-PDP) block copolymers with two types of thiolation degree, 5.04% (B-SH5%) and 10.5% (B-SH11%), were prepared. The PDP introduction rates were calculated from the peak intensity ratio of the methylene protons of PEG (OCH_2CH_2, $\delta = 3.7$ ppm) to the pyridyl protons of the PDP group (C_5H_4N, $\delta =$ 7.0−8.5 ppm) measured by ^1H NMR as typically seen in Figure 1B (B-SH5%).

Conjugation of c(RGDfK) peptide ligands into the PEG terminus of acetal-PEG-P(Lys-PDP) was achieved through the formation of a thiazolidine ring between an N-terminal cysteine and an aldehyde group converted from the acetal group.[11] The acetal group was deprotected under moderate acidic conditions to the aldehyde group. To avoid an exchange reaction between the thiol group of cysteine residue in the c(RGDfK) peptide and the pyridylthio group in the acetal-PEG-P(Lys-PDP), the pyridylthio group was deprotected with DTT prior to the installation of the ligand. After the dialysis against the AcOH buffer to remove excessive DTT as well as to convert the acetal group to an aldehyde group, the c(RGDfK) peptide was added to react with the aldehyde-PEG-P(Lys-MP) in AcOH buffer, resulting in the introduction of the peptide ligand. This type of conjugation between the N-terminal cysteine and the aldehyde group occurs selectively even in the presence of primary amines, since the conjugation through a Schiff base between a primary amine and the aldehyde group is reversible, whereas the conjugation through a thiazolidine ring between the N-terminal cysteine and the aldehyde group is irreversible. The methyl protons of the acetal group ($\delta = 1.2$ ppm) and the aromatic protons of the pyridylthio group ($\delta = 7.0-8.5$ ppm) completely disappeared with the appearance of protons assigned to the aromatic ring of D-phenylalanine (f: D-Phe) ($\delta = 7.3$ and 7.4 ppm) in the c(RGDfK) (Figure 1C). Based on the peak intensity ratios of the aromatic protons of the peptide ligands to the methylene protons of PEG ($\delta = 3.7$ ppm), the introduction rates of the peptide ligands in the c(RGDfK)-PEG-P(Lys-MP) were determined to be 73% and 87% for the B-SH5% and the B-SH11%, respectively.

Formation of Polyplex Micelles. Agarose gel electrophoresis showed that free pDNA was not detected in the polyplex micelles at N/P = 2 (data not shown), confirming that all of the pDNA were entrapped in polyplex micelles. Ellman's test revealed that less than 2% of the thiol groups in the polyplex micelles were free (data not shown), suggesting that almost all of the thiol groups seem to be involved in the formation of disulfide bonds. These results are consistent with our previous report.[9] The sizes, shapes, and ζ-potentials of the cross-linked polyplex micelles were evaluated by DLS, AFM, and laser-doppler electrophoresis, respectively. Table 1 summarizes the cumulant diameters and ζ-potentials of the polyplex micelles at N/P = 2. The cumulant diameters of all the micelles were approximately 110 nm with a moderate polydispersity index between 0.14 and 0.18, regardless of the composition of the thiolated polymers or the introduction of RGD ligands. Also, the ζ-potentials of all the micelles were kept at slightly positive values between +1.1 and +3.6, which is consistent with the formation of the PEG palisade surrounding the polyplex core.[6,18] Figure 2 shows AFM images of B-SH11% cross-linked micelles with or without RGD ligands, where a toroidal structure in the size range of 60−100 nm and a rodlike structure with a long axis of 160−200 nm were observed, corresponding to the sizes from DLS. These results suggest that the physicochemical characteristics of the polyplex micelles are quite similar regardless of the thiolation degree or the introduction of RGD ligands.

Table 1. Size and ζ-Potential of Polyplex Micelles (N/P = 2) with or without Cyclic RGD Peptide Ligands

thiolation degree (%)	cyclic RGD peptide ligand	cumulant diameter (nm)/ polydispersity index (μ/Γ^2)	ζ-potential (mV)
0	(−)	109 ± 0.75/0.169 ± 0.002	1.47 ± 0.312
	(+)	113 ± 1.11/0.156 ± 0.004	2.27 ± 0.148
5	(−)	115 ± 0.71/0.141 ± 0.007	1.62 ± 0.348
	(+)	106 ± 0.48/0.144 ± 0.009	3.57 ± 0.230
11	(−)	111 ± 0.25/0.145 ± 0.011	1.15 ± 0.788
	(+)	114 ± 1.08/0.172 ± 0.005	1.52 ± 0.213

Transfection. The *in vitro* transfection efficiencies of B-SH0%, B-SH5%, and B-SH11% polyplex micelles with or without RGD ligands were evaluated for HeLa cells possessing $\alpha_v\beta_3$ and $\alpha_v\beta_5$ integrin receptors (Figure 3A). A cyclic RGD peptide is well-known to selectively recognize $\alpha_v\beta_3$ and $\alpha_v\beta_5$ integrins among several integrins.[19] In the transfection experiments with non-cross-linked micelles (B-SH0% micelle), the introduction of RGD ligands led to approximately doubled transfection efficiency. Notably, RGD (+) B-SH5% and RGD (+) B-SH11% micelles with cross-

(18) Harada-Shiba, M.; Yamauchi, K.; Harada, A.; Takamisawa, I.; Shimokado, K.; Kataoka, K. Polyion Complex Micelles as Vectors in Gene Therapy-Pharmacokinetics and In Vivo Gene Transfer. *Gene Ther.* **2002**, *9*, 407–414.

(19) Haubner, R.; Gratias, R.; Difenbach, B.; Goodman, S. L.; Jonczyk, A.; Kessler, H. Structual and Functional Aspects of RGD-Containing Cyclic Pentapeptides as Highly Potent and Selective Integrin $\alpha_v\beta_3$ Antagonists. *J. Am. Chem. Soc.* **1996**, *118*, 7461–7472.

linked cores and RGD ligands showed 10-fold higher efficiency than the ligand-less system without cross-linking (RGD (−) B-SH0% micelle). It is obvious that the effect of ligand installation was drastically enhanced by introducing disulfide cross-linking in the core. RGD (+) B-SH5% polyplex micelles achieved the highest transfection efficiency. Consequently, the combination of core cross-linking and ligand installation enhanced efficiency 20 times more than the polyplex micelles without ligands and cross-links.

Then, to further confirm that the increased transfection efficiency by RGD (+) micelles involves the receptor-mediated mechanism, a competitive assay using free cyclic RGD peptides was carried out for B-SH11% cross-linked micelles (Figure 3B). RGD (+) micelles showed a remarkably high transfection efficiency compared with RGD (−) micelles in the absence of free cyclic RGD peptides ($P < 0.01$). As the concentration of free cyclic RGD peptides increased, the transfection efficiency of RGD (+) micelles accordingly decreased, approaching the transfection level of RGD (−) micelles under the condition of 100 μM cyclic RGD peptides ($P = 0.104$). Thus, the results of the competitive assay indicate that $\alpha_v\beta_3$ and/or $\alpha_v\beta_5$ integrin receptor-mediated endocytosis is involved in the transfection of the RGD (+) micelles against HeLa cells.

Analysis of Cellular Uptake of Polyplex Micelles. In general, the enhanced transfection by ligands has been attributed to an increased uptake of vectors.[14,20,21] Thus, the cellular uptake of the RGD (−) and RGD (+) micelles into the HeLa cells was evaluated using a system loaded with ^{32}P-labeled pDNA (Figure 3C). Regardless of ligand installation, cross-linked micelles tend to be taken up more efficiently than noncrosslinked micelles. The introduction of disulfide cross-links into the micelle core appreciably contributes to an increase in the stability of micelles under physiological conditions.[9] This implies that disulfide cross-links might prevent the micelles from dissociation in the extracellular medium, and consequently facilitate their internalization into the cellular compartment. Interestingly, there is no significant increase in micelle uptake even by installing RGD ligands, suggesting that other factors, including modulation of intracellular trafficking, may be involved in the enhancement of transfection efficiency by cyclic RGD peptide ligands.

Intracellular Distribution of Polyplex Micelles. Our previous report showed that RGD (+) polyplex micelles preferentially localize in the perinuclear region, unlike RGD (−) polyplex micelles,[11] suggesting that RGD ligands likely modulate intracellular trafficking of polyplex micelles. Therefore, detailed observation of the intracellular distribution was carried out using CLSM (Figure 4). The medium was replaced with fresh medium after 1 h incubation of polyplex micelles with cultured HeLa cells. Then CLSM observation was carried out after each reincubation without polyplex micelles in the medium. The CLSM images are shown in Figure 4A. The micelles localized in the inner-cytoplasm were quantitatively evaluated using the procedure described in the Experimental Section and shown in Figure 4B; the data are summarized in Figure 4C. After the 5 h reincubation (total 6 h incubation), the spots observed in the inner region of the cytoplasm were mainly the green spots of RGD (+) micelles (Figure 4A, left). On the other hand, the RGD (−) micelles, shown in red stayed mainly near the cell membrane (Figure 4A, left), but some fraction was observed in the inner-cytoplasm as red spots (RGD (−) micelle alone) or yellow spots (colocalizing with RGD (+) micelles). In the early stages, almost half of the cell population with fluorescence had only green spots, corresponding to the internalization of RGD (+) micelles (Figure 4C); this indicated that RGD (+) micelles were internalized into the inner-cytoplasm much faster than RGD (−) micelles. However, further reincubation resulted in the decrease in the cell fraction that showed only green spots and lead to an increase in the fraction that included yellow spots, corresponding to the colocalization of RGD (−) and RGD (+) micelles, as well as to an increase in red spots, corresponding to the presence of RGD (−) micelles alone. Note that there are two possibilities for the appearance of yellow spots. The first is that RGD (−) and RGD (+) micelles adsorbing to the cell membrane were simultaneously endocytosed by the cell. The second is that RGD (−) and RGD (+) micelles that were separately internalized into the cells subsequently colocalized through the possible fusion of the compartments in the inner-cytoplasm. On the other hand, the green spots still existed in a definite fraction of cells (G + GY + GRY) even after long-term reincubation, while the fraction of the cells including red spots (R + RY + GRY) continued to increase (Figure 4C). Thus, it is reasonable to assume that there may be distinct routes of internalization for RGD (−) and RGD (+) micelles, and eventually their final destinations may be different.

To examine whether or not RGD ligand installation in the micelles alters their intracellular trafficking, organelles were selectively stained using LysoTracker for the late endosomes and the lysosomes, and CT-B for the lipid rafts and the caveosomes (Figures 5 and 6).[22,23] In this experiment, the medium was replaced 1 h after the addition of polyplex micelles, followed by 11 h of reincubation. The rate of colocalization was quantified by the formula shown in the Experimental Section. The experiment with LysoTracker revealed that 39% of RGD (−) micelles and 28% of RGD (+) micelles in the inner-cytoplasm were localized in the late endosomes and lysosomes, indicating that the colocalization ratio of RGD (−) micelles with the late endosomes and lysosomes was significantly higher than that of RGD (+) micelles ($P = 0.0052$) (Figure 5B). On the other hand, the observation with CT-B revealed that 22% of RGD (−)

(20) de Bruin, K.; Ruthardt, N.; von Gersdorff, K.; Bausinger, R.; Wagner, E.; Ogris, M.; Bräuchle, C. Cellular Dynamics of EGF Receptor-Targeted Synthetic Viruses. *Mol. Ther.* **2007**, *15*, 1297–1305.

(21) Vinogradov, S.; Batrakova, E.; Li, S.; Kabanov, A. Polyion Complex Micelles with Protein-Modified Corona for Receptor-Mediated Delivery of Oligonucleotides into Cells. *Bioconjugate Chem.* **1999**, *10*, 851–860.

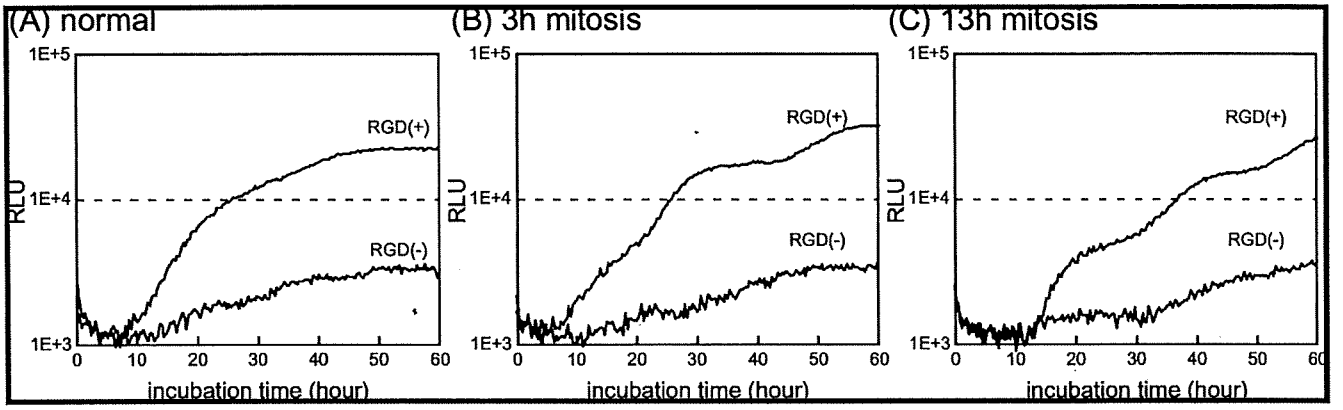

Figure 7. Real-time luciferase gene expression of B-SH11% polyplex micelles (N/P = 2) with or without cyclic RGD peptide ligands under the "normal" condition (A), the "3 h mitosis" condition (B), and the "13 h mitosis" condition (C).

micelles and 44% of RGD (+) micelles in the inner-cytoplasm were localized in the lipid rafts and caveosomes, respectively, indicating that the RGD (+) micelles had significantly higher localization ratios to the lipid rafts and caveosomes than the RGD (−) micelles ($P = 0.0004$) (Figure 6B). These results indicate that the polyplex micelles with cyclic RGD ligands were internalized preferentially through caveolae-mediated endocytosis by HeLa cells.

Real Time Luciferase Gene Expression. In the conventional luciferase assay, transfected cells need to be lysed before measurement, and this restricts the evaluation of luciferase expression in real time. Alternatively, as explained in the Experimental Section, Kronos Dio allows us to measure real-time luciferase expression while maintaining the cell culture for a prolonged period.[24] Figure 7 shows the results of time-dependent gene expression with RGD (−) and RGD (+) B-SH11% micelles. Under the "normal" condition without any control over the cell cycle (Figure 7A), the luciferase expression with RGD (−) and RGD (+) micelles started almost simultaneously around 8 h after the micelles were added. The expression of genes reached a plateau after around 50 h of incubation regardless of the presence of RGD ligands. Considering that the half-life of luciferase is about 2−3 h in living cells,[25] the rate of luciferase production is expected to be equal to that of luciferase degradation in regions over 50 h. RGD (+) micelles showed higher transfection rates than RGD (−) micelles at all time points. Real-time gene expression was assessed for cells after aphidicolin, a DNA synthesis inhibitor, was used to synchronize the cell cycle (Figures 7B and 7C). HeLa cells incubated with aphidicolin for more than 16 h are arrested between the G1 and S phases,[17] and a change to a medium that dose not contain aphidicolin allows HeLa cells to progress into the S phase to divide 13 h later. We confirmed that almost all HeLa cells were in the S phase immediately after the medium replacement and were in the G2 phase 10 h after the replacement (data not shown). Under the "3 h mitosis" condition, where cell division started 3 h after polyplex micelles were added (Figure 7B), gene expression by RGD (+) micelles was detected 5 h after incubation, while that of RGD (−) micelles was below the Kronos Dio detection limit even after about 12 h of incubation. This implies that RGD (+) micelles can migrate into the nucleus during the first mitosis due to their early accumulation in the perinuclear region, whereas this is not the case for RGD (−) micelles because of their slow accumulation in that region. Under the "13 h mitosis" condition, where cell division started 13 h after polyplex micelles were added (Figure 7C), luciferase expression with RGD (−) and RGD (+) micelles was detected simultaneously at 13 h after incubation, which corresponds to the initiation of cell division. This result suggests that RGD (+) micelles move early to the perinuclear region but may not be actively transported into the nucleus in the nonmitotic condition. As shown in Figure 4, most of the RGD (−) micelles were internalized into the cell to accumulate in the perinuclear region at a level comparable to that of RGD (+) micelles after 24 h of incubation. Nevertheless, RGD (−) micelles under the "13 h mitosis" condition exhibited remarkably lower increases in luciferase expression at more than 30 h of incubation compared to RGD (+) micelles. Apparently, this cannot be explained by the difference in the migration rate between RGD (−) and RGD (+) micelles because of their similar levels of accumulation in the perinuclear region in this time period. Presumably, this might be explained by the difference in the final destinations of the polyplex micelles with and without cyclic RGD ligands due to the modulation of intracellular trafficking as shown in Figures 5 and 6.

(22) Orlandi, P. A.; Fishman, P. H. Filipin-Dependent Inhibition of Cholera Toxin: Evidence for Toxin Internalization and Activation through Caveolae-Like Domains. *J. Cell Biol.* **1998**, *141*, 905–915.

(23) von Gersdorff, K.; Sanders, N. N.; Vandenbroucke, R.; de Smedt, S. C.; Wagner, E.; Ogris, M. The Internalization Route Resulting in Successful Gene Expression Depends on both Cell Line and Polyethylenimine Polyplex Type. *Mol. Ther.* **2006**, *14*, 745–753.

(24) Takae, S.; Miyata, K.; Oba, M.; Ishii, T.; Nishiyama, N.; Itaka, K.; Yamasaki, Y.; Koyama, H.; Kataoka, K. PEG-Detachable Polyplex Micelles Based on Disulfide-Linked Block Catiomers as Bioresponsive Nonviral Gene Vectors. *J. Am. Chem. Soc.* **2008**, *130*, 6001–6009.

(25) Ignowski, J. M.; Schaffer, D. V. Kinetic Analysis and Modeling of Firefly Luciferase as a Quantitative Reporter Gene in Live Mammalian Cells. *Biotechnol. Bioeng.* **2004**, *86*, 827–834.

Discussion

In the present study, two distinctive implementations, that of environment-sensitive cross-links in the core and that of cyclic RGD peptide ligands on the surface, were integrated into the polyplex micelles formed by PEG-PLys block copolymers and pDNA. The physicochemical characteristics of these micelles were quite similar regardless of the thiolation degree or the introduction of RGD ligands (Table 1). The PEG palisade surrounding the polyplex core shielded the charges of the micelles to maintain very small absolute values in the ζ-potentials. The cumulant diameter of polyplex micelles was around 100 nm. This indicates that all of the polyplex micelles possess favorable characteristics relevant to future *in vivo* application. In transfection experiments using cultured cells, polyplex micelles with cyclic RGD ligands achieved higher transfection efficiency than polyplex micelles without cyclic RGD ligands against HeLa cells appreciably expressing $\alpha_v\beta_3$ integrin receptors (Figure 3A). Interestingly, RGD ligands' effect on transfection was further enhanced by the introduction of disulfide cross-linking in the micelle core. Disulfide cross-links have been reported to stabilize polyplex micelles against the counter polyanion exchange reaction under nonreductive conditions.[9] Therefore, cross-linked micelles might acquire greater stability in the medium compared to noncrosslinked micelles, indicating the enhanced effect of cyclic RGD ligands. Note that RGD (+) B-SH5% micelles achieved the highest transfection efficiency among all micelles. Excessive cross-linking into the cores of polyplex micelles has been reported to overstabilize the micelles and impede the release of pDNA,[9] which is considered to be a cause of the lower transfection efficiency of B-SH11% micelles compared to that of B-SH5% micelles. The inhibitory experiment using free cyclic RGD peptides (Figure 3B) certainly confirmed that receptor-mediated uptake by RGD ligands contributed to the enhancement of gene expression. It is worth noting that the enhancement was not due to an increase in the cellular uptake of polyplex micelles (Figure 3C), suggesting that cyclic RGD peptide ligands may modulate the intracellular trafficking of the polyplex micelles, leading to increased transfection efficiency. In this regard it should be noted that, in our previous study, cyclic RGD ligands facilitated the transport of the polyplex micelles to the perinuclear region.[11] Other studies found that some ligands, such as b-FGF[26] and lactose,[27] contribute to the change in the intracellular trafficking of gene vectors. Time-dependent CLSM observation revealed that RGD (+) micelles were internalized into the cytoplasm and moved to the perinuclear region much earlier than RGD (−) micelles (Figure 4). This is consistent with the results of real-time luciferase expression under the "3 h mitosis" condition, where RGD (+) micelles exhibited earlier onset of gene expression with high efficiency (Figure 7B). The CLSM observation also clarified the variation in final localization in the cytoplasm between the two micelles (Figure 4). CLSM observation with the staining of acidic endosomes and lysosomes (Figure 5) or lipid rafts and caveosomes (Figure 6) revealed that RGD (+) micelles were distributed in the acidic organelles at lower levels than RGD (−) micelles, and were preferentially internalized via caveolae-mediated endocytosis. Considering that pDNA degradation occurs in late endosomes and lysosomes by enzymatic hydrolysis, RGD (+) micelles are more likely than RGD (−) micelles to protect entrapped pDNA from enzymatic degradation. It is known that cells uptake particles of different sizes through different routes: macropinocytosis (>200 nm), clathrin-mediated endocytosis (100−200 nm), and caveolae-mediated endocytosis (<100 nm).[28] The average particle size of RGD (−) and RGD (+) micelles was around 110 nm, with a moderate size distribution (polydispersity index = 0.14−0.18). Thus, these micelles are likely to be internalized by both clathrin- and caveolae-mediated endocytosis. Also, cyclic RGD peptides selectively recognize both $\alpha_v\beta_3$ and $\alpha_v\beta_5$ integrin receptors. $\alpha_v\beta_5$ integrins, which adenoviruses use for their internalization into target cells, are known to facilitate clathrin-mediated endocytosis,[29] while $\alpha_v\beta_3$ integrin-mediated internalization occurs via caveolae-mediated endosytosis.[30,31] Since $\alpha_v\beta_3$ integrins have 10-times higher binding affinity to cyclic RGD peptides than $\alpha_v\beta_5$ integrins,[32] it is reasonable to assume that RGD (+) micelles might preferably recognize $\alpha_v\beta_3$ integrins and thus to induce the caveolae-mediated endocytosis as the internalization route into HeLa cells. Alternatively, RGD (−) micelles, based on their size, might be primarily internalized by clathrin-mediated endocytosis and subsequently delivered to the acidic compartment of a lysosome. Caveolae-mediated endocytosis is not associated with a pH decrease, and is

(26) Fisher, K. D.; Ulbrich, K.; Subr, V.; Ward, C. M.; Mautner, V.; Blankey, D.; Seymour, L. W. A Versatile System for Receptor-Mediated Gene Delivery Permits Increased Entry of DNA into Target Cells, Enhanced Delivery to the Nucleus and Elevated Rates of Transgene Expression. *Gene Ther.* **2000**, *7*, 1337–1343.

(27) Hashimoto, M.; Morimoto, M.; Saimoto, H.; Shigemasa, Y.; Sato, T. Lactosylated Chitosan for DNA Delivery into Hepatocytes: The Effect of Lactosylation on the Physicochemical Properties and Intracellular Trafficking of pDNA/Chitosan Complexes. *Bioconjugate Chem.* **2006**, *17*, 309–316.

(28) Grosse, S.; Aron, Y.; Thevenot, G.; Francois, D.; Monsigny, M.; Fajac, I. Potocytosis and Cellular Exit of Complexes as Cellular Pathways for Gene Delivery by Polycations. *J. Gene Med.* **2005**, *7*, 1275–1286.

(29) Wickman, T. J.; Filardo, E. J.; Cheresh, D. A.; Nemerow, G. R. Integrin $\alpha_v\beta_5$ Selectively Promotes Adenovirus Mediated Cell Membrane Permeabilization. *J. Cell Biol.* **1994**, *127*, 257–264.

(30) Wary, K. K.; Mainiero, F.; Isakoff, S. J.; Marcantonio, E. E.; Giancotti, F. G. The Adaptor Protein Shc Couples a Class of Integrins to the Control of Cell Cycle Progression. *Cell* **1996**, *87*, 733–743.

(31) Wary, K. K.; Mariotti, A.; Zurzolo, C.; Giancotti, F. G. A Requirement for Caveolin-1 and Associated Kinase Fyn in Integrin Signaling and Anchorage-Dependent Cell Growth. *Cell* **1998**, *94*, 625–634.

(32) Marinelli, L.; Gottschalk, K.-E.; Meyer, A.; Novellino, E.; Kessler, H. Human Integrin $\alpha_v\beta_5$: Homology Modeling and Ligand Binding. *J. Med. Chem.* **2004**, *47*, 4166–4177.

known to be a nondigestive route of external substances into the cellular compartment.[33] Some nonenveloped viruses, such as simian virus 40, utilize this route for transfection to host cells and accumulate in a smooth endoplasmic reticulum compartment.[34,35] Thus, RGD (+) micelles internalized by caveolae-mediated endocytosis may be able to avoid pDNA degradation in acidic organelles, leading to high transfection efficiency. Moreover, as seen in the real-time luciferase assay under the "13 h mitosis" condition (Figure 7C), the luciferase expression of RGD (+) micelles detected at 30 h was remarkably higher than that of RGD (−) micelles, despite the comparable levels of cellular uptake between the two (Figures 3C and 4). Obviously, this result cannot be explained by the difference in the migration rate, because there was sufficient time for both RGD (+) and RGD (−) micelles to accumulate in the perinuclear region before mitosis. The higher gene expression of RGD (+) micelles is consistent with their preferential localization in caveosomes due to distinctive intracellular trafficking through the nonacidic and nondegradable route of caveolae-mediated endocytosis.

It should be noted that the results in Figures 5 and 6 indicate that not all of the RGD (+) micelles were internalized by caveolae-mediated endocytosis. Clathrin-mediated endocytosis, a relatively slow uptake pathway, could also contribute to the internalization of a portion of RGD (+) micelles, possibly due to the nonspecific interaction between the micelle and the cell membrane, even though polyplex micelles are covered with PEG to minimize nonspecific interaction. Nevertheless, the ζ-potentials of the polyplex micelles still take small positive values, suggesting that PEG charge shielding is incomplete. This slight positive charge might induce the nonspecific interaction of polyplex micelles with the negatively charged cell membrane. If this is the case, an increase in the PEG density of polyplex micelles may reduce the interaction, increasing the ligand's effects on the uptake and gene expression of polyplex micelles. An alternative explanation on the nonspecific uptake of polyplex micelles is available by considering the amphiphilic character of the PEG molecule. A PEG chain under concentrated conditions, as found in the shell layer in the micelle system, might have the ability to interact with the plasma membrane components through hydrophobic interaction or indirectly through a bridge of hydrated water molecules.[36] Research to clarify the underlying mechanism is now under way in our laboratory, and the results will be reported elsewhere in the near future.

Conclusions

In conclusion, polyplex micelles with integrated implementations of cyclic RGD peptide ligands on the micelle surface and disulfide cross-linking in the core achieved remarkably enhanced transfection efficiency against HeLa cells expressing $\alpha_v\beta_3$ integrins on the surface. The RGD ligands were effective not for increasing uptake but for modulating intracellular trafficking of polyplex micelles. RGD (+) micelles were distributed in the perinuclear region at an early period and were preferentially internalized by caveolae-mediated endocytosis via nonacidic and nondegradable intracellular compartments. These results indicate that polyplex micelles with cyclic RGD ligands and disulfide cross-links are promising approaches to facilitate cell-specific transfection by controlling intracellular trafficking as well as by the environment-sensitive release of encapsulated pDNA in the target cells.

Cyclic RGD peptide is well-known to selectively recognize $\alpha_v\beta_3$ integrin receptors identified as a marker of angiogenic vascular tissue,[37] and thus is a good candidate as a ligand for gene vectors used for diseases including tumor characterized by neovascularization. Indeed, nonviral gene vectors, in which cyclic RGD peptide ligands are installed have been applied to delivery pDNA and siRNA to tumor vasculature, effectively suppressing tumor growth.[13,14] Thus, polyplex micelle with cyclic RGD ligands and disulfide cross-links may be a useful system for cancer gene therapy through a systemic administration.

Acknowledgment. This work was financially supported in part by the Core Research Program for Evolutional Science and Technology (CREST) from Japan Science and Technology Corporation (JST), by Special Coordination Funds for Promoting Science and Technology (SCF) commissioned by the Ministry of Education, Culture, Sports, Science, and Technology (MEXT) of Japan, and by Grant-in-Aid for Nanomedicine Research from the Ministry of Health, Labour and Welfare (MHLW), Japan.

MP800070S

(33) Pelkmans, L.; Kartenbeck, J.; Helenius, A. Caveolar Endocytosis of Simian Virus 40 Reveals a New Two-Step Vesicular-Transport Pathway to the ER. *Nat. Cell Biol.* **2001**, *3*, 473–483.

(34) Norkin, L. C.; erson, H. A.; Wolfrom, S. A.; Oppenheim, A. Caveolar Endocytosis of Simian Virus 40 Is Followed by Brefeldin A-Sensitive Transport to the Endoplasmic Reticulum, Where the Virus Disassembles. *J. Virol.* **2002**, *76*, 5156–5166.

(35) Conner, S. D.; Schmid, S. L. Regulated Portals of Entry into the Cell. *Nature* **2003**, *422*, 37–44.

(36) Kataoka, K.; Kwon, G. S.; Yokoyama, M.; Okano, T.; Sakurai, Y. Block Copolymer Micelles as Vehicles for Drug Delivery. *J. Controlled Release* **1993**, *24*, 119–132.

(37) Brooks, P. C.; Clark, R. A.; Cherish, D. A. Requirement of Vascular Integrin $\alpha_v\beta_3$ for Angiogenesis. *Science* **1994**, *264*, 569–571.

Enhancement of Angiogenesis Through Stabilization of Hypoxia-inducible Factor-1 by Silencing Prolyl Hydroxylase Domain-2 Gene

Shourong Wu[1,2], Nobuhiro Nishiyama[1,3], Mitsunobu R Kano[3,4], Yasuyuki Morishita[4], Kohei Miyazono[4], Keiji Itaka[1], Ung-il Chung[1,3,5] and Kazunori Kataoka[1,3,6]

[1]Division of Clinical Biotechnology, Center for Disease Biology and Integrative Medicine, Graduate School of Medicine, The University of Tokyo, Tokyo, Japan; [2]Department of Chemistry and Biotechnology, Graduate School of Engineering, The University of Tokyo, Tokyo, Japan; [3]Center for NanoBio Integration, The University of Tokyo, Tokyo, Japan; [4]Department of Molecular Pathology, Graduate School of Medicine, The University of Tokyo, Tokyo, Japan; [5]Department of Bioengineering, Graduate School of Engineering, The University of Tokyo, Tokyo, Japan; [6]Department of Materials Engineering, Graduate School of Engineering, The University of Tokyo, Tokyo, Japan

Hypoxia-inducible factor-1 (HIF-1) plays a central role in cellular response to hypoxia by activating vascular endothelial growth factor (VEGF) and other angiogenic factors. Prolyl hydroxylase domain-2 (PHD2) protein induces the degradation of HIF-1 by hydroxylating specific prolyl residues. Therefore gene silencing of PHD2 by RNA interference (RNAi) might increase the expression of angiogenic growth factors and, consequently, neoangiogenesis through the stabilization of HIF-1α. In this study we have shown that the specific silencing of PHD2 is sufficient for stabilizing HIF-1α and increasing its transcriptional activity, resulting in the increased expression of angiogenic factors including VEGF and fibroblast growth factor-2 (FGF2). Moreover, when PHD2-siRNA vector was used, the increase in VEGF secretion was observed for as long as 18 days after transfection. *In vitro* treatment of human umbilical vein endothelical cells with conditioned medium from PHD2-siRNA vector-transfected NIH3T3 cells was shown to increase cell proliferation. Also, *in vivo* angiogenesis was observed in mice implanted with Matrigel plugs mixed with NIH3T3 cells transfected with PHD2-siRNA vector. These results indicate that PHD2 silencing induces expressions of multiple angiogenic growth factors by stabilizing HIF-1α, and that the implantation of cells transfected with PHD2-siRNA vector is sufficient to enhance angiogenesis *in vivo*. In the light of these findings, PHD2 silencing by RNAi might offer a potential tool for angiogenic therapy.

Received 9 October 2007; accepted 7 April 2008; published online 20 May 2008. doi:10.1038/mt.2008.90

INTRODUCTION

Therapeutic angiogenesis aims to improve neovascularization in ischemic tissues by delivery of angiogenic factors or DNA vectors encoding those proteins, such as vascular endothelial growth factor (VEGF) and fibroblast growth factor-2 (FGF2).[1–3] VEGF is produced in the early stage of the angiogenic cascade and is responsible for the initial activation of endothelial cells; this makes it an important factor in vascular development.[4] Its transgenic expression in mouse skin results in increased numbers of blood vessels that manifest excessive permeability.[5] FGF2 has been reported to act as a mitogen for both endothelial and mural cells,[6] and its role in vascular formation has also been identified.[3,7] Therapeutic angiogenesis using either VEGF or FGF2 alone has been extensively investigated. However, although phase I clinical trials had shown that their delivery was safe, phase II trials have not demonstrated efficacy as expected,[8–10] thereby suggesting that the administration of a single angiogenic growth factor might be insufficient to induce functional vessels. Therapeutic angiogenesis studies were then altered to focus on the combined application of angiogenic growth factors. The combination of VEGF and FGF2, and the combinations of each of these with other angiogenic factors such as angiopoietin-1 and platelet-derived growth factor-BB (PDGF-BB), have been reported to have potent synergistic effects on neovascularization, in both *in vitro* and *in vivo* experiments.[11–15] Collectively, these results demonstrate the complexity of the mechanism of angiogenesis, which includes the temporally and spatially orchestrated expression of multiple angiogenic factors.

Hypoxia-inducible factor-1 (HIF-1), a heterodimeric α, β transcription factor, functions as a central regulator of oxygen homeostasis, and is known to be hydroxylated on two proline residues by prolyl hydroxylase domain (PHD) prolyl hydroxylase family and degraded by E3 ubiquitin ligase complex under normoxia conditions. The inactivation of PHD2, a member of the PHD family, contributes to HIF stabilization, thereby suggesting that PHD2 is the key HIF prolyl hydroxylase.[16] More than 60 HIF-1 target genes, including VEGF and other angiogenic factors, have been identified.[17] In this context, transgenic expression of HIF-1α in mouse skin was shown to increase vascularization without excessive permeability,[18] and the expression of its constitutively active form is sufficient to induce angiogenesis in nonischemic tissue.[19]

Correspondence: Kazunori Kataoka, Department of Materials Engineering, Graduate School of Engineering, The University of Tokyo, 7-3-1 Hongo, Bunkyo-ku, Tokyo 113-8656, Japan. E-mail: kataoka@bmw.t.u-tokyo.ac.jp

RNA interference (RNAi) is a post-transcriptional gene-silencing phenomenon triggered by double-stranded RNA discovered in 1998 (ref. 20). Owing to its great specificity and efficiency, RNAi has become a powerful tool in studying gene functions, and has been extensively investigated as a therapeutic tool.[21,22] Several therapy applications are currently under clinical development.[23,24]

In this study we explored the potential for therapeutic angiogenesis using PHD2-suppressing RNAi. We demonstrated *in vitro* that PHD2 silencing upregulates the expression of multiple angigogenic growth factors. We also showed that *in vivo* implantation of PHD2-silenced cells is sufficient to enhance angiogenesis in an experimental animal model. These results have implications for the application of PHD2-suppressing RNAi in therapeutic angiogenesis.

RESULTS

Construction of pshRNAs against murine PHD2, and PHD2 gene silencing

The RNAi effect of small-interfering RNA (siRNA) is highly dependent on the sequence of the target gene. Therefore we selected two siRNAs with different sequences[25,26] and a siPHD2-pool containing four kinds of PHD2-suppressing siRNAs. All the PHD2-suppressing siRNAs clearly showed suppressive effects, with siPHD2-A showing the strongest such effect (**Figure 1a**). In order to further determine their functional effect, we investigated the efficacy of siPHD2s on HIF-1 transcriptional activity. Under normoxia conditions, both siPHD2-A-transfected NIH3T3 and C2C12 cells exhibited a significant increase in HIF-1 transcriptional activity (**Supplementary Figure S1a and b**). Consistently, in term of increasing VEGF mRNA level and protein secretion, siPHD2-A was more potent than the others (**Supplementary Figures S2 and S3**). Consistent with the decrease of its suppressive effect at 72 hours after transfection (**Figure 1a**), the effect of siPHD2 on the increase of VEGF secretion also decreased at 96 hours after transfection (**Supplementary Figure S3**). In order to obtain a long-term silencing effect, we constructed the siPHD2 expression vectors U6-pshPHD2-A, U6-pshPHD2-B, CMV-pshPHD2-A, and CMV-pshPHD2-B. U6-pshPHD2-A and CMV-psh-PHD2-A suppressed the expression of PHD2 mRNA more potently (**Figure 1b** and **c**, 90 and >60%, respectively) than the U6-shPHD2-B and CMV-psh-PHD2-B did (60 and >40%, respectively). Next, using a 5× hypoxia-responsive element promoter-driven firefly luciferase reporter (5×HRE reporter), we investigated the effect of PHD2- and PHD3 silencing on HIF-1 transcriptional activity. Under normoxia conditions, the transcriptional activity of HIF-1 was induced by pshPHD2-A vectors but not by pshPHD3 vectors (**Figure 1d** and **e**). Moreover, because U6 promoter-driven siPHD2 expression vectors showed more potent suppressive effects and induction of HIF-1 transcriptional activity than those using a cytomegalovirus (CMV) promoter, we used U6-pshPHD2-A for performing further *in vitro* and *in vivo* experiments. In addition, the suppressive effect on PHD2 by U6-pshPHD2-A persisted at>90% at 72 hours after transfection (**Figure 1f**), thereby indicating that, for achieving long-term effects, pshRNA expression vector was more potent than siRNA.

Effects of PHD2 silencing on HIF-1α protein level and HIF-1 transcriptional activity

In a normoxia environment, hydroxylation of HIF-1α protein by PHD2 resulted in the proteasomal degradation of HIF-1α.[27] This finding confirmed the effect of PHD2 silencing on HIF-1α protein. HIF-1α protein increased significantly in PHD2-silenced cells as compared to control cells (**Figure 2a**). Consistent with the earlier report, the results also showed that PHD2 silencing did not affect HIF-2α protein levels (**Figure 2a**).[16] Moreover, PHD2 silencing did not alter HIF-1α distribution in nuclei and cytoplasm (**Figure 2a** and **b**, respectively); rather, it increased the amount of HIF-1α protein in the nuclei predominantly, and an even greater increase was observed in PHD2-silenced cells exposed to conditions of hypoxia (**Figure 2c**). That is, the transcriptional activity of HIF-1 was higher when PHD2 was silenced, under both normoxia and hypoxia conditions (**Figure 2d**).

Regulation of expression of various angiogenic growth factors by silencing of PHD2

Next we analyzed whether PHD2 silencing could regulate the expression of multiple genes encoding angiogenic growth factors. The endogenous HIF-1α mRNA level in PHD2-silenced cells

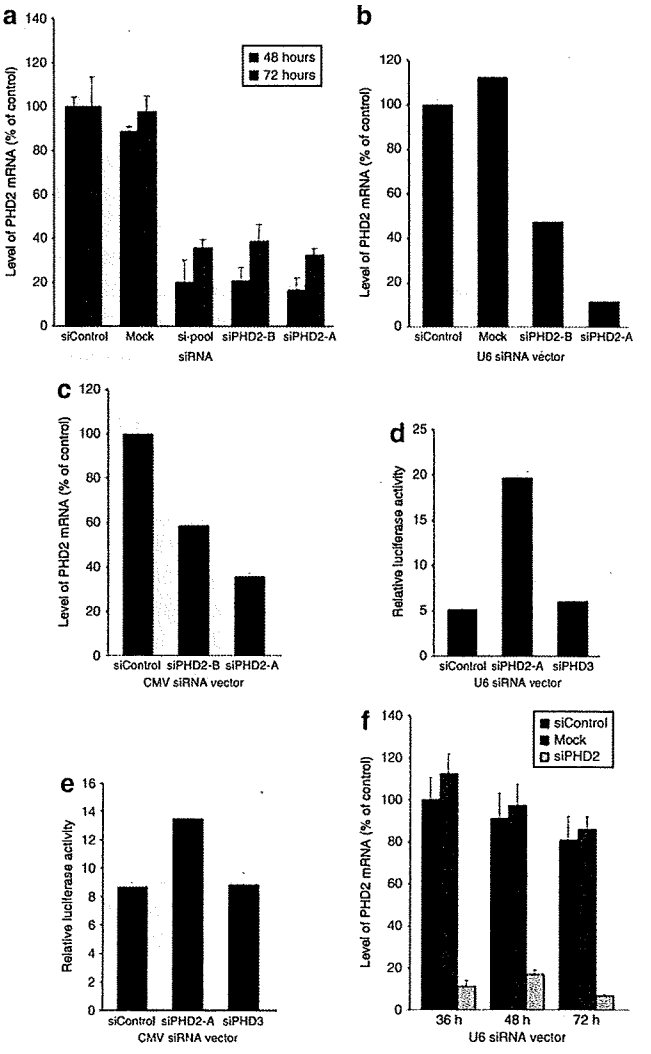

was not different from that in control cells (**Figure 3a**). In addition, procollagen PHD2, a member of another prolyl 4-hydroxylase family, was also not influenced by pshPHD2 vector- or siRNA-induced PHD2 silencing (**Figure 3b** and **Supplementary Figure S4**). However, the mRNA levels of angiogenic growth factor genes, *i.e.*, VEGF, FGF2, and angiopoietin-1, were significantly increased (**Figure 3c–e**), while the expression level of PDGF-B was not altered (data not shown). These results indicate that the increase in VEGF, FGF2, and angiopoietin-1 induced by PHD2 silencing might be caused by the stabilization of HIF-1α rather than by the increase in HIF-1α mRNA expression.

Effect of PHD2 silencing on VEGF secretion

As shown in **Figure 4a**, the amount of VEGF secreted was significantly higher in PHD2-silenced cells than in control cells. Consistent with the higher suppressive effect of U6-pshPHD2-A, the level of VEGF secretion from cells transfected with U6-pshPHD2-A was higher than that from cells transfected with U6-pshPHD2-B. Moreover, the silencing effect of U6-pshPHD2-A on PHD2 as well as the increased level of VEGF secretion persisted for at least 18 days (**Figure 4b** and **c**).

PHD2 silencing promotes proliferation of HUVECs

We next investigated whether PHD2 silencing could increase endothelial cell proliferation. For this purpose, we first investigated the effect of PHD2 silencing on NIH3T3 cells. PHD2 silencing resulted in an increased proliferation of NIH3T3 cells (**Figure 5a**), probably because of the increase in the levels of growth factors, especially FGF2, which could also have the effect of enhancing the growth of fibroblast cells. We next determined the effect of the conditioned media from NIH3T3 cells on the proliferation of human umbilical vein endothelial cells (HUVECs). HUVECs treated with conditioned medium from PHD2-silenced cells showed significant increase in growth as compared to those treated with conditioned medium from controls (**Figure 5b**).

PHD2 silencing enhances angiogenesis *in vivo*

In order to test further whether PHD2 silencing is also effective in neoangiogenesis *in vivo*, we carried out the *in vivo* Matrigel plug assay as described earlier.[13] The results are shown in **Figure 6**. The areas shown in green represent the endothelium of vasculature, with the predominant linear structures indicating small vessels and some apparently circular structures indicating larger vessels. Structures double-positive for green (PECAM1) and red (SMA) (merged to yellow) indicate vessels with pericyte coverage, which are more mature vessels. Matrigel plugs mixed with NIH3T3 cells transfected with siPHD2-A exhibited slightly more neovascularization than those mixed with the cells transfected with control siRNA (**Figure 6a**). H and E staining also confirmed the results (**Figure 6a**, left). Next we investigated the effect of the U6-pshPHD2-A vector on neoangiogenesis. Matrigel plugs mixed with NIH3T3 cells transfected with U6-pshPHD2-A vector exhibited potent angiogenesis, with more pericyte-covered (and therefore more mature) neovasculature (**Figure 6b**), whereas Matrigel plugs mixed with cells transfected with control U6-pshRNA vector or mock cells exhibited almost no neoangiogenesis. The results of H and E staining also revealed that the U6-pshPHD2-A vector enhances neoangiogenesis, with tubelike structures containing red blood cells (arrowheads) exhibiting functional vasculature (**Figure 6b**, left). The quantification of mature neovasculature as revealed by the Matrigel plug assay, determined on the basis of pericyte-covered endothelium (vascular structures that are double-positive for SMA and PECAM), confirmed that PHD2 silencing, especially by the shPHD2 vector, enhances the induction of mature vasculature (**Figure 7**). The neoangiogenesis effect induced by the U6-pshPHD2-A vector resulted in an approximately fourfold increase in mature neovasculature, while the neoangiogenesis effect induced by the PHD2 siRNA resulted in only a twofold increase.

DISCUSSION

Therapeutic angiogenesis is a strategy involving the use of angiogenic molecules to induce the development of new blood vessels. However, because the clinical application of either recombinant VEGF or FGF2 by itself showed a less significant effect than expected,[8–10] the focus of therapeutic angiogenesis shifted to treatment using combinations of angiogenic molecules.[11–15] We have already confirmed that the combination treatment with recombinant VEGF and FGF2 has a synergistic effect on angiogenesis.[13] It follows, therefore, that a master regulator capable of simultaneously regulating multiple angiogenic growth factors might be a better choice for the target of gene therapy. An example of this kind of regulator is HIF-1, which plays an important role in angiogenesis by coordinately regulating the expression of multiple

Figure 1 Knockdown effect of prolyl hydroxylase domain-2 (PHD2)-suppressing small-interfering RNAs (siRNAs) and siRNA expression vectors on endogenous PHD2 mRNA expression and hypoxia inducible factor-1 (HIF-1) transcriptional activity. (**a**) The suppressive effect of PHD2-suppressing siRNAs on the endogenous PHD2 mRNA expression level in NIH3T3 cells. Cells were transfected with PHD2-suppressing siRNAs. Forty-eight and seventy-two hours after transfection, real-time reverse transcriptase-PCR (RT-PCR) analysis was performed. Nontargeting siRNA was used as control, and nontransfected cells at each time-point were also shown as mock. The data shown represent mean values ± SD, $n = 3$. (**b**) The effect of PHD2-suppressing U6-pshRNA expression vectors on endogenous PHD2 in NIH3T3 cells. Total RNA was collected from nontransfected cells and from cells transfected with the indicated U6-pshPHD2 expression vector or control U6 pshRNA expression vector, and real-time RT-PCR was performed. The results were normalized to the actin mRNA expression level, and shown relative to values from cells transfected with control vector. The data shown represent mean value ± SD, $n = 3$. (**c**) The effect of PHD2-suppressing CMV-pshRNA expression vectors on endogenous PHD2 in NIH3T3 cells. Real-time RT-PCR analysis was performed as described earlier. (**d–e**) The induction effect of PHD2 silencing on HIF-1 transcriptional activity in NIH3T3 cells. The cells were cotransfected with control vectors, or (**d**) the indicated U6 pshRNA expression vectors, or (**e**) CMV-pshRNA expression vectors, hypoxia-response reporter vector (5× hypoxia-responsive element promoter driven firefly luciferase reporter) and *Renilla* luciferase vector (pRL-SV40). Forty-eight hours later, dual luciferase assay was performed, and the results were normalized to the *Renilla* luciferase expression level. The data shown represent mean values ± SD, $n = 3$. (**f**) The suppressive effect of U6-pshPHD2-A expression vector on the endogenous PHD2 mRNA in NIH3T3 cells. The cells were transfected with U6-pshPHD2-A or control vector, selection was carried out, and real-time RT-PCR was performed to quantify PHD2 expression at the indicated time-points; nontransfected cells at each time-point were shown as mock. The results were normalized to the actin expression level and shown relative to the values from cells transfected with control vector. The data shown represent mean value ± SD, $n = 3$. shRNA, short-hairpin RNA.

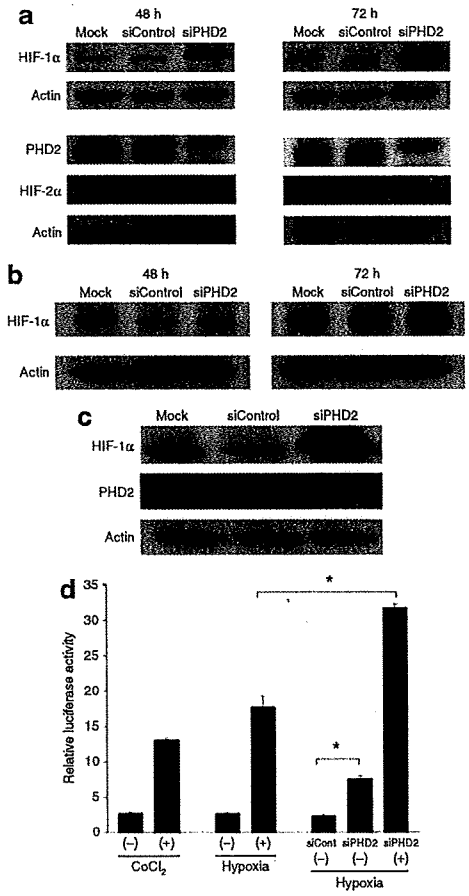

Figure 2 Prolyl hydroxylase domain-2 (PHD2) silencing induced stabilization of endogenous hypoxia-inducible factor-1α (HIF-1α) and increased HIF-1α transcriptional activity. (**a**) NIH3T3 cells were transfected with U6-pshPHD2-A or with control U6 vector, and Western blotting analysis was performed for detection of HIF-1α, HIF-2α, and PHD2 in the nuclei under normoxia conditions at the indicated time-points. Nontransfected cells were also shown as mock. Actin was used as a loading control. (**b**) Western blotting analysis of HIF-1α in the cytoplasm of cells transfected with U6 pshRNA expression vector and mock cells under normoxia conditions at the indicated time-points. (**c**) Western blotting analysis for detection of HIF-1α and PHD2 in the nuclei of cells transfected with U6 pshPHD2 expression vector or control vector, and mock cells under hypoxia conditions. NIH3T3 cells transfected with U6 pshRNA expression vectors were plated under hypoxia conditions (1% O_2) for 6 hours, and the nuclei extract of the cells was subjected to Western blotting analysis. (**d**) Effect of PHD2 silencing on the induction of HIF-1 transcriptional activity in cells exposed to $CoCl_2$ (a hypoxia-mimicking reagent), normoxia, or hypoxia conditions. NIH3T3 cells transfected with control siRNA vector or U6-pshpHD2-A vector were cotransfected with 5× hypoxia-responsive element promoter driven firefly luciferase reporter and *Renilla* luciferase vector, and then exposed to medium alone, medium containing $CoCl_2$ (100 μmol/l), or hypoxia conditions (1% O_2). Six hours later, dual luciferase assays were performed. The silencing of PHD2 significantly induced HIF-1 transcriptional activity under both normoxia ($^*P < 0.05$) and hypoxia conditions ($^*P < 0.05$), as compared to their respective controls. Results were normalized to the activity level of *Renilla* luciferase expression. The data shown represent mean value ± SD, $n = 3$. shRNA, short-hairpin RNA.

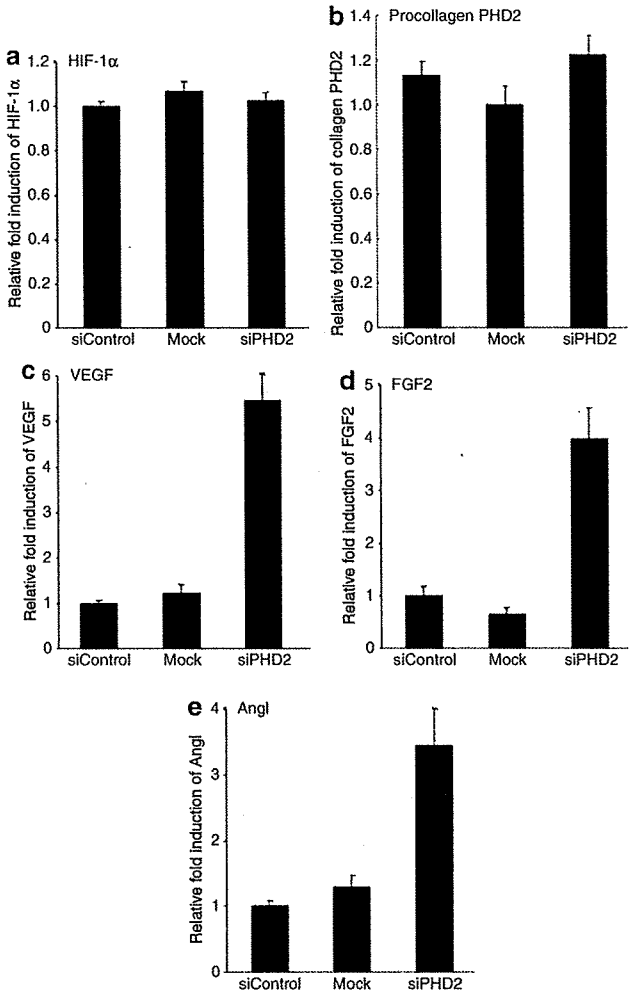

Figure 3 Effect of prolyl hydroxylase domain-2 (PHD2) silencing on angiogenic growth factor expression. NIH3T3 cells were transfected with U6-pshPHD2-A or with control vector, selection was carried out at 48 hours, and total RNA was isolated and subjected to real-time reverse transcriptase-PCR analysis: (**a**) hypoxia inducible factor-1α (HIF-1α); (**b**) procollagen PHD2; (**c**) vascular endothelial growth factor (VEGF); (**d**) fibroblast growth factor-2 (FGF2); and (**e**) angiopoietin-1 (Ang1). Nontransfected cells were also shown as mock. The results were normalized to the mRNA expression level of actin and shown relative to cells transfected with control. The data shown represent mean value ± SD, $n = 3$.

genes encoding critical angiogenic growth factors in a cell type–specific manner.[19] By virtue of its ability to upregulate multiple genes, HIF-1α has become an attractive molecular target for the treatment of ischemic or postischemic tissue injury.

Our results show that PHD2 silencing can functionally protect HIF-1α protein from proteasomal degradation and induce multiple angiogenic growth factors (VEGF, FGF2, and angiopoietin-1). However, to date, the *cis*-acting hypoxia-response elements (HIF-1 binding sites) have not been demonstrated in the regulatory regions of those angiogenic growth factor genes (except in VEGF). It remains to be determined, therefore, whether their regulation by HIF-1α is direct or indirect. Notably, we could not detect any obvious increase in the mRNA level of PDGF-B in NIH3T3 cells. This may be attributed to the fact that the regulation of angiogenic growth factors by HIF-1α is remarkably cell type–specific.[19] However, it is still possible that this silencing may induce the development of functional vessels. As shown in **Figure 3**, PHD2 silencing induced upregulation of both VEGF and FGF-2 in NIH3T3 cells. This result is consistent with the earlier report[13] showing that

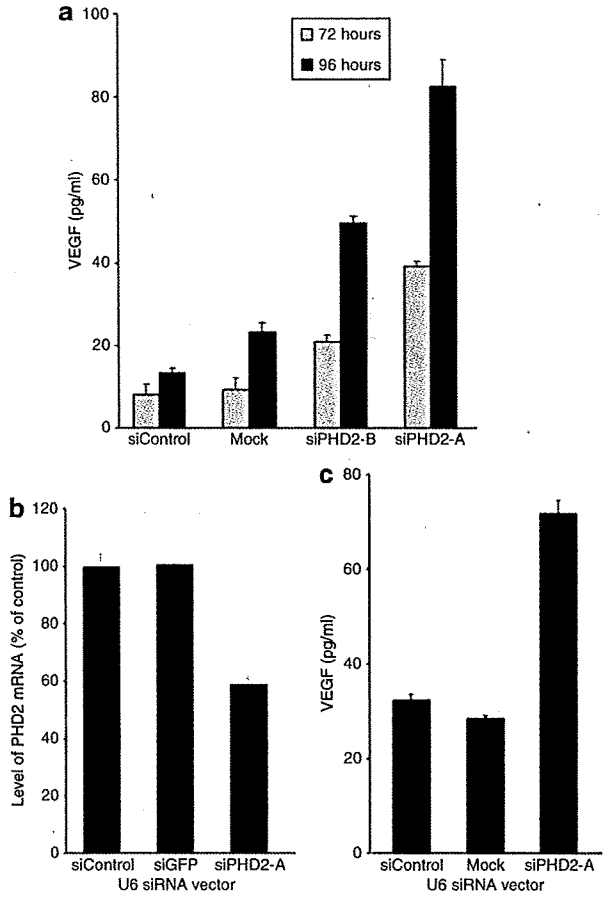

Figure 4 The induction effect of prolyl hydroxylase domain-2 (PHD2) silencing on the secretion of vascular endothelial growth factor (VEGF). NIH3T3 cells were transfected with U6-pshPHD2 vectors or with control vector for the indicated durations. (**a**) Quantification analysis of VEGF protein level in culture medium of cells transfected with U6-pshPHD2 vectors or control vector, and nontransfected cells (mock) by enzyme-linked immunosorbent assay (ELISA). (**b–c**) Long-term silencing effect of U6-pshPHD2-A in transfected cells 18 days after transfection: Real-time reverse transcriptase-PCR (RT-PCR) analysis was performed for the detection of PHD2 mRNA expression levels (**b**) and ELISA was performed for the detection of VEGF protein level in culture medium (**c**). The results of the real-time RT-PCR analysis were normalized to the mRNA expression level of actin, and shown relative to cells transfected with control vector. The data shown represent mean value ± SD, $n = 3$.

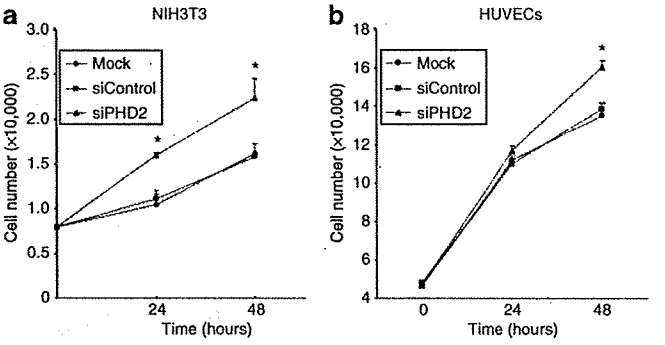

Figure 5 Prolyl hydroxylase domain-2 (PHD2) silencing promotes proliferation of NIH3T3 cells and human umbilical vein endothelial cells (HUVECs). (**a**) NIH3T3 cells transfected with U6-pshPHD2-A or with control vector were cultured further for the indicated durations, and cell numbers were counted. Nontransfected cells were also shown as mock. (**b**) HUVECs were cultured under serum-starved conditions, with conditioned medium obtained from U6-psh-PHD2-A- or control vector-transfected NIH3T3 cells or mock cells, and cell numbers were counted. Assays were performed in triplicate. The data shown represent mean value ± SD.

a combination of VEGF and FGF2 could synergistically induce more mature neovasculature through enhancement of endogenous PDGF-BB expression from endothelium, thereby gathering more pericytes to the endothelium through an enhanced gradient of PDGF-BB. Our results also showed that PHD2 silencing affects the proliferation of both NIH3T3 and HUVEC cells. This observation could be attributable to the increased expression of growth factors that induce signal-promoting cell proliferation. These results are consistent with published data showing that overexpression of PHD2 suppresses endothelial cell proliferation.[25]

In agreement with the earlier study,[28] our experiments showed that U6-pshPHD2 exhibited a stronger silencing effect than the CMV-pshPHD2 vector, thereby confirming that, at least at present, the U6 promoter (an RNA polymerase III promoter) is one of the most suitable promoters for expressing siRNAs, given its strong transcription activity[29] and absence of any extra sequence such as 5′-Cap and 3′-poly A.[28] We also confirmed that the pshPHD2 expression vector is more potent in inducing angiogenesis *in vivo* than the siRNA of the same target sequence. This might be because of the short half-life of siRNA, on account of degradation by intracellular RNase. Consequently, the continuous release of angiogenic growth factors for a long period, which is important for successful angiogenesis, could not be obtained. In general, therefore, two different approaches can be utilized for therapeutic applications: siRNA expression vectors for achieving middle- and long-term knockdown effect, and siRNAs for achieving short-term effect.

We have demonstrated, for the first time, that siRNA against PHD2 (HIF PHD2) can effectively induce neoangiogenesis by coordinately regulating the expression of multiple angiogenic growth factors through the stabilization of HIF-1α. Recently, Natarajan *et al.* showed that siRNA against procollagen prolyl 4-hydroxylase-2 (GenBank accession no. NM_011031, referred to also as "PHD2" mistakenly in their report, but in reality a different gene), can attenuate myocardial ischemia reperfusion injury and stabilize HIF-1α.[30] The phenotype they observed might be associated with the procollagen prolyl 4-hydroxylases-iNOS pathway, and not with the HIF prolyl hydroxylase/HIF/angiogenic growth factor pathway. Additionally, consistent with our results, Takeda *et al.*, using a conditional knockout mouse model, identified the role of HIF PHD2 in the adult vascular system.[31]

Earlier reports showed that, although the induction of angiogenesis using only VEGF does result in a vascular response, the induced vessel is unphysiologically permeable because of the absence of other external growth factors.[32] Direct expression of HIF-1α or HIF-1α lacking oxygen-sensitive degradation domain for angiogenesis has also been reported,[19,33] indicating that HIF-1α might be a good target for angiogenesis. However, the exogenous high and persistent expression of HIF1α[19] or oxygen-sensitive degradation domain–deficient HIF-1α[33] might result in some side effects such as development of cancers. Short-hairpin RNAs (shRNAs), expressed using nonviral vectors and synthetic siRNAs

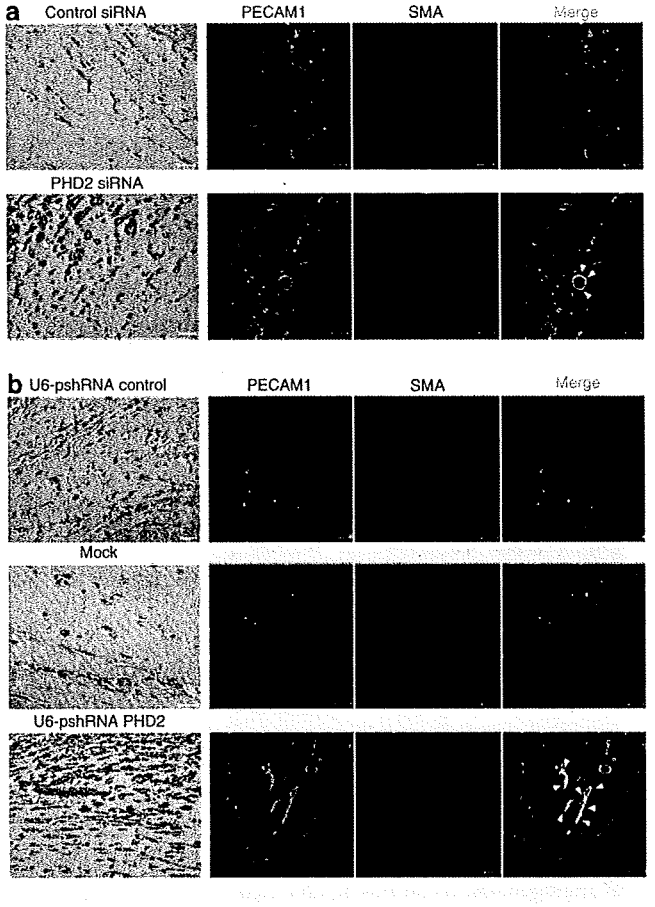

Figure 6 Prolyl hydroxylase domain-2 (PHD2) silencing enhances neoangiogenesis in a Matrigel plug assay *in vivo*. NIH3T3 cells transfected with (**a**) siPHD2-A, or (**b**) U6-psh-PHD2-A or their controls were mixed with Matrigel and injected subcutaneously into the abdominal region of 5-week-old female Balb/c mice ($n = 3$–5). After 7 days, the gels were excised and subjected to hematoxylin and eosin (H&E) staining (**a** and **b** left panels; scale bars = 40 μm), and to immunohistochemistry with anti-PECAM1 (shown in green, representing endothelium) and anti-SMA (shown in red, those adjacent to endothelium representing pericytes) (scale bars = 50 μm). Representative data from each experiment are shown. (**a**) Matrigel plug assay using cells transfected with siPHD2-A. siRNA-induced PHD2-silencing exhibited slightly more endothelium as compared to the control, with some of it covered by pericytes (arrow heads), (**a**: upper panels). (**b**) Matrigel plug assay using cells transfected with U6-psh-PHD2-A. U6-psh-PHD2-A vector-induced PHD2 silencing exhibited significantly more endothelium, with most of it covered by pericytes (arrowheads in immunohistochemistry) or more vessels containing red blood cells (arrowheads in H&E staining), as compared to the controls (**b**: upper panels) and to those mixed with cells transfected with siPHD2-A (**a**: lower panel). PECAM1, platelet-endothelial cell adhesion molecule-1; SMA, smooth muscle actin.

that are modified to enhance their stability, are potentially advantageous because of their temporary effect. PHD inhibitors have also been being explored as potential therapeutic agents; however, they are likely to lack adequate specificity. As shown in **Figure 3b** and **Supplementary Figure S4**, silencing of HIF-PHD2 has no influence on procollagen PHD2. Therefore, given its high specificity and strong effect, RNAi might be a better choice in therapeutic applications. Indeed, RNAi-based therapeutic applications have been in clinical trials for some diseases,[34,35] and some other preclinical trials are under development.[36–38]

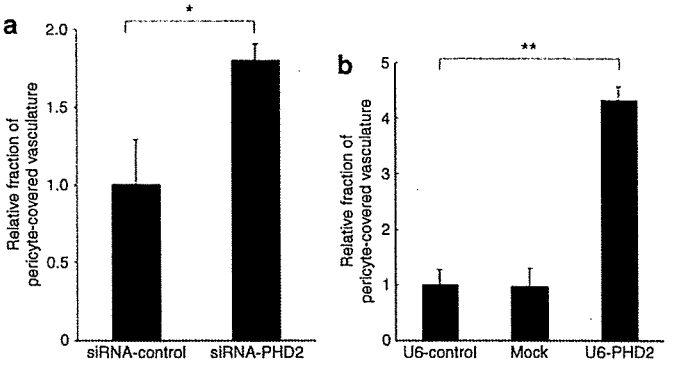

Figure 7 Quantification of the formation of new vessels in Matrigel plugs. (**a**) Quantification in Matrigel plug assay using cells transfected with siPHD2-A, and (**b**) quantification in Matrigel plug assay using cells transfected with U6-psh-PHD2-A. The quantification of the fraction of the pericyte-covered vasculature in whole neovasculature was performed by measuring the ratio of platelet-endothelial cell adhesion molecule-1 (PECAM1) to smooth muscle actin double-positive area (yellow area) within the PECAM1 area (green area), based on the immunohistochemistry results ($n = 9$). $^*P < 0.05$; $^{**}P < 0.01$. PHD2, prolyl hydroxylase domain-2; siRNA, small-interfering RNA.

In this study, we have demonstrated that implantation of PHD2-silenced cells is sufficient to enhance neoangiogenesis *in vivo*. These results could provide a basis for further therapeutic application, *i.e.*, using PHD2-suppressing RNAi as a potential strategy for angiogenic therapy. However, because of the limitation of our *in vivo* method, some further issues need to be addressed: (i) systematic evaluations on the basis of the functional aspects of regenerated vessels, including vascular hyperpermeability; (ii) additional preclinical and clinical studies, particularly in respect of safety and efficacy for therapeutic use in patients with ischemic cardiovascular diseases such as myocardial infarction; (iii) the development of delivery systems to deliver the siRNA expression vector and/or siRNA to the target sites and to make them functional in an efficient and safe manner. In this regard, we have explored polymeric micelle-based nanocarriers for plasmid DNA[39,40] and siRNA,[41,42] and demonstrated their *in vitro* and *in vivo* efficacies, including efficient gene transfer to primary cells,[40] *in vivo* transfection to a rabbit carotid artery,[43] and transfection-mediated bone regeneration.[44] We intend to further investigate the use of these nanocarriers in PHD2-silencing-mediated neoangiogenesis therapy.

MATERIALS AND METHODS

Cell lines and culture. The mouse fibroblast cells NIH3T3 (Riken Cell Bank, Tsukuba, Japan) were cultured in Dulbecco's modified Eagle's medium (Sigma-Aldrich, St. Louis, MO) containing 10% fetal bovine serum (Sigma-Aldrich). HUVECs (Lonza, Walkersville, MD) were maintained in the angiogenic medium EBM2 plus EGM2 (Lonza).

Preparation of siRNA expression vectors. siRNAs of murine PHD2 and PHD3 (GenBank accession no. NM_053207 and NM_028133, respectively) were synthesized (Dharmacon, Lafayette, Colorado). The sense sequences of DNA corresponding to murine PHD2-duplex siRNAs were 5′-GAACTCAAGCCCAATTCAG-3′ (siPHD2-A) and 5′-TGAG CGAGCGAGAGCTAAA-3′ (siPHD2-B). The sense sequence of DNA corresponding to murine PHD3-duplex siRNAs was 5′-GGCAAT GGTGGCTTGCTAT-3′. The SMART pool siRNAs of murine PHD2 and nontargeting siRNA containing 21 nucleotide sequences with no homology

to murine genes, which was used for control (NTSC), were also purchased from Dharmacon. Luciferase reporter gene assays were carried out using plasmid DNA encoding luciferase driven by the 5× hypoxia-responsive element (5×HRE) promoter, kindly supplied by Dr. Kondo of the Graduate School of Medicine, Kyoto University. The shRNA expression vectors were constructed by placing oligonucleotides based on the two siRNAs of murine PHD2 and PHD3 (mentioned earlier) into pSilencer 2.1-U6 or pSilencer 4.1-CMV (nos. 5762 and 5775, respectively; Ambion, Austin, TX) in accordance with the manufacturer's instructions.

Transient transfections and dual luciferase reporter assays. NIH3T3 cells were seeded in 24-well dishes at 1.5×10^5 cells/dish. The next day, the cells were cotransfected with the indicated siRNA expression vectors, 5×HRE reporter and *Renilla* luciferase expression vector (pRL-SV40, Promega), using FuGENE6 reagent (Roche Applied Science, Mannheim, Germany). Twenty-four hours after cotransfection, the cells were exposed to either medium alone, or medium containing $CoCl_2$ (100 μmol/l), and then incubated for 6 hours so as to chemically stabilize HIF-1α. For the hypoxia-environment experiment, 24 hours after cotransfection the siRNA vector-transfected NIH3T3 cells were plated into an Anaeropouch Box (1% O_2; Mitsubishi GAS chemical Company, Tokyo, Japan) and cultured for 6 hours. Dual luciferase assays were then performed using the Dual Luciferase Assay System (Promega). Relative luciferase activities were determined by calculating the ratio between the activity levels of firefly and *Renilla* luciferase. The results are shown as mean value ± SD ($n = 3$). For siRNA experiments, NIH3T3 cells were first transfected with the indicated siRNA for 12 hours using Lipofectamine 2000 (Invitrogen, Carlsbad, CA), and then cotransfected with 5×HRE reporter and *Renilla* luciferase expression vectors. Dual luciferase assays were performed 24 hours later.

Quantitative RT-PCR analysis. RNA was purified using TRIZOL reagent and the RNeasy column (Invitrogen). Total RNA (1 μg) treated with DNase I (Qiagen, Hilden, Germany) was reverse transcribed using QuantiTect Reverse Transcription (Qiagen), and real-time RT-PCR was performed using the ABI 7500 Fast Real-time RT-PCR System (Applied Biosystems, Foster City, CA) and QuantiTect SYBR Green PCR Master Mix (Qiagen). All reactions were run in triplicate. All expression data were normalized to actin. The sequences of the primers used are listed in **Supplementary Table S1.**

Western blot analysis. Whole cells were collected by centrifugation. The separation of nuclear and cytoplasmic extract was performed using an NE-PER Kit (Pierce, Rockford, IL). Sample proteins were electrophoresed on sodium dodecyl sulfate polyacrylamide gel electrophoresis and transferred to a polyvinylidene fluoride membrane (Bio-Rad, Hercules, CA). Western blottings were performed as described earlier.[45] Primary antibodies against mouse HIF-1α (NB100-449; Novus Biological, Littleton, CO), HIF-2α (NB100-122; Novus), PHD2 (NB100-2219; Novus), and actin (Sigma-Aldrich) were used for detecting the corresponding protein.

Enzyme-linked immunosorbent assay. NIH3T3 cells were transfected with the indicated siRNAs or siRNA expression vectors. For siRNA vector-transfected cells, a selection was carried out 24 hours after transfection so as to eliminate the untransfected cells. The transfected cells were seeded onto 24-well plates. Culture supernatants were harvested at the indicated time-points. VEGF was measured using a commercially available sandwich immunoassay kits (MMV00; R&D Systems, Minneapolis, MN).

Cell viability assays. HUVECs were seeded into collagen I–coated 24-well culture plates at a density of 3×10^4 cells/well. After 24 hours, the medium was changed to Dulbecco's modified Eagle's medium containing 1% fetal bovine serum and 20% conditioned medium, and plates were again incubated at 37°C in 5% CO_2. The viable cells were counted 24 and 48 hours after additional culture, using colorimetric assays with 2-(2-methoxy-4-nitrophenyl)-3-(4-nitrophenyl)-5-(2,4-disulphophenyl)-2H-tetrazolioum monosodium salt (Cell Counting Kit-8; Dojindo, Kumamoto, Japan) in accordance with the manufacture's instructions. For cell viability assays in NIH3T3 cells, the cells transfected by the siRNA control expression vector and those transfected by the siPHD2 expression vector were seeded into 48-well culture plates at a density of 8,000 cells/well in Dulbecco's modified Eagle's medium. After 24 and 48 hours, live cells were counted as described earlier.

In vivo *Matrigel plug assay.* NIH3T3 cells were transfected with siRNA expression vector of murine PHD2 (pSilencer 2.1-U6 puro) using FuGENE6 (Roche Applied Science). After 24 hours, selection was performed with puromycin so as to eliminate untransfected cells. Two days later, the selected cells were harvested. 1.0×10^6 NIH3T3 cells were mixed with regular Matrigel (BD Biosciences, Bedford, MA). The Matrigels (400 μl each) were injected subcutaneously into the abdominal region of female Balb/c mice (CLEA Japan, Tokyo, Japan). Each mouse was injected with one implant. Each experiment performed on three to five mice. The Matrigel plugs were removed on day 7, and were either directly frozen in dry-iced acetone for immunohitochemistry or fixed with formalin and paraffin-embedded for H&E staining. For the Matrigel plug assay mixed with siRNA-transfected cells, NIH3T3 cells were mixed with Matrigel and injected into the mice 24 hours after transfection with control siRNA and PHD2 siRNA. All experiment protocols were conducted in accordance with the policies of the Animal Ethics Committee at the University of Tokyo.

Immunohistochemistry of Matrigel plugs. The frozen matrigel plugs were sliced into sections of 10 μm thickness using a cryostat. The fixed sections were incubated with antimurine PECAM1 (Clone Mec13.3; BD Pharmingen 553730, BD Biosciences Pharmingen, San Diego, CA) for 1 hour. The specimens were subsequently stained with antirat/IgG conjugated with Alexa Fluor 488 (Invitrogen Molecular Probes) and monoclonal antimurine α-SMA Cy3 conjugate (Sigma-Aldrich) for 1 hour at room temperature. Confocal laser scanning analysis was performed using an LSM 510 microscope (Carl Zeiss, Germany) at an excitation wavelength of 488 and 543 nm.

Quantification in Matrigel plug assays. We quantified the formation of mature vessel structures in Matrigel plugs by measuring the ratio of the PECAM1 area to the SMA-postive (yellow) area within the PECAM1-postive (green) area using LSM image software (Carl Zeiss), yielding the fraction of endothelial-positive structures that are co-positive for smooth muscle structures. Microsoft Excel software was used for statistical analysis. The data represent average values from nine areas from three independent Matrigel plugs.

ACKNOWLEDGMENTS

This work was supported by the Core Research Program for Evolutional Science and Technology from the Japan Science and Technology Agency, and Grants-in-Aid for Scientific Research from the Japanese Ministry of Education, Culture, Sports, Science and Technology. The authors declare that they have no conflict of interest.

SUPPLEMENTARY MATERIAL

Figure S1. PHD2-silencing via siRNAs induced HIF-1 transcriptional activity in NIH3T3 cells and C2C12 cells.
Figure S2. PHD2-silencing via siRNAs induced VEGF mRNA expression in NIH3T3 cells.
Figure S3. PHD2-silencing via siRNAs induced the secretion of VEGF.
Figure S4. The influence of PHD2-silencing induced siRNA on procollagen PHD2.
Table S1. Primers used for real-time RT-PCR.

REFERENCES

1. Olsson, AK, Dimberg, A, Kreuger, J and Claesson-Welsh, L (2006). VEGF receptor signalling - in control of vascular function. *Nat Rev Mol Cell Biol* **7**: 359–371.

2. Shibuya, M and Claesson-Welsh, L (2006). Signal transduction by VEGF receptors in regulation of angiogenesis and lymphangiogenesis. *Exp Cell Res* **312**: 549–560.
3. Magnusson, P, Rolny, C, Jakobsson, L, Wikner, C, Wu, Y, Hicklin, DJ *et al.* (2004). Deregulation of Flk-1/vascular endothelial growth factor receptor-2 in fibroblast growth factor receptor-1-deficient vascular stem cell development. *J Cell Sci* **117**: 1513–1523.
4. Carmeliet, P, Ferreira, V, Breier, G, Pollefeyt, S, Kieckens, L, Gertsenstein, M *et al.* (1996). Abnormal blood vessel development and lethality in embryos lacking a single VEGF allele. *Nature* **380**: 435–439.
5. Detmar, M, Brown, LF, Schon, MP, Elicker, BM, Velasco, P, Richard, L *et al.* (1998). Increased microvascular density and enhanced leukocyte rolling and adhesion in the skin of VEGF transgenic mice. *J Invest Dermatol* **111**: 1–6.
6. Bikfalvi, A, Klein, S, Pintucci, G and Rifkin, DB (1997). Biological roles of fibroblast growth factor-2. *Endocr Rev* **18**: 26–45.
7. Lee, SH, Schloss, DJ and Swain, JL (2000). Maintenance of vascular integrity in the embryo requires signaling through the fibroblast growth factor receptor. *J Biol Chem* **275**: 33679–33687.
8. Simons, M, Annex, BH, Laham, RJ, Kleiman, N, Henry, T, Dauerman, H *et al.* (2002). Pharmacological treatment of coronary artery disease with recombinant fibroblast growth factor-2: double-blind, randomized, controlled clinical trial. *Circulation* **105**: 788–793.
9. Henry, TD, Annex, BH, McKendall, GR, Azrin, MA, Lopez, JJ, Giordano, FJ *et al.* (2003). The VIVA trial: Vascular endothelial growth factor in Ischemia for Vascular Angiogenesis. *Circulation* **107**: 1359–1365.
10. Lederman, RJ, Mendelsohn, FO, Anderson, RD, Saucedo, JF, Tenaglia, AN, Hermiller, JB *et al.* (2002). Therapeutic angiogenesis with recombinant fibroblast growth factor-2 for intermittent claudication (the TRAFFIC study): a randomised trial. *Lancet* **359**: 2053–2058.
11. Pepper, MS, Ferrara, N, Orci, L and Montesano, R (1992). Potent synergism between vascular endothelial growth factor and basic fibroblast growth factor in the induction of angiogenesis *in vitro*. *Biochem Biophys Res Commun* **189**: 824–831.
12. Asahara, T, Bauters, C, Zheng, LP, Takeshita, S, Bunting, S, Ferrara, N *et al.* (1995). Synergistic effect of vascular endothelial growth factor and basic fibroblast growth factor on angiogenesis *in vivo*. *Circulation* **92**: II365–II371.
13. Kano, MR, Morishita, Y, Iwata, C, Iwasaka, S, Watabe, T, Ouchi, Y *et al.* (2005). VEGF-A and FGF-2 synergistically promote neoangiogenesis through enhancement of endogenous PDGF-B-PDGFRbeta signaling. *J Cell Sci* **118**: 3759–3768.
14. Richardson, TP, Peters, MC, Ennett, AB and Mooney, DJ (2001). Polymeric system for dual growth factor delivery. *Nat Biotechnol* **19**: 1029–1034.
15. Cao, R, Brakenhielm, E, Pawliuk, R, Wariaro, D, Post, MJ, Wahlberg, E *et al.* (2003). Angiogenic synergism, vascular stability and improvement of hind-limb ischemia by a combination of PDGF-BB and FGF-2. *Nat Med* **9**: 604–613.
16. Appelhoff, RJ, Tian, YM, Raval, RR, Turley, H, Harris, AL, Pugh, CW *et al.* (2004). Differential function of the prolyl hydroxylases PHD1, PHD2, and PHD3 in the regulation of hypoxia-inducible factor. *J Biol Chem* **279**: 38458–38465.
17. Semenza, GL (2003). Targeting HIF-1 for cancer therapy. *Nat Rev Cancer* **3**: 721–732.
18. Elson, DA, Thurston, G, Huang, LE, Ginzinger, DG, McDonald, DM, Johnson, RS *et al.* (2001). Induction of hypervascularity without leakage or inflammation in transgenic mice overexpressing hypoxia-inducible factor-1α. *Genes Dev* **15**: 2520–2532.
19. Kelly, BD, Hackett, SF, Hirota, K, Oshima, Y, Cai, Z, Berg-Dixon, S *et al.* (2003). Cell type-specific regulation of angiogenic growth factor gene expression and induction of angiogenesis in nonischemic tissue by a constitutively active form of hypoxia-inducible factor 1. *Circ Res* **93**: 1074–1081.
20. Fire, A, Xu, S, Montgomery, MK, Kostas, SA, Driver, SE and Mello, CC (1998). Potent and specific genetic interference by double-stranded RNA in *Caenorhabditis elegans*. *Nature* **391**: 806–811.
21. Hannon, GJ and Rossi, JJ (2004). Unlocking the potential of the human genome with RNA interference. *Nature* **431**: 371–378.
22. Paddison, PJ, Silva, JM, Conklin, DS, Schlabach, M, Li, M, Aruleba, S *et al.* (2004). A resource for large-scale RNA-interference-based screens in mammals. *Nature* **428**: 427–431.
23. Leung, RK and Whittaker, PA (2005). RNA interference: from gene silencing to gene-specific therapeutics. *Pharmacol Ther* **107**: 222–239.
24. Behlke, MA (2006). Progress towards *in vivo* use of siRNAs. *Mol Ther* **13**: 644–670.
25. Takeda, K and Fong, GH (2007). Prolyl hydroxylase domain 2 protein suppresses hypoxia-induced endothelial cell proliferation. *Hypertension* **49**: 178–184.
26. Busca, R, Berra, E, Gaggioli, C, Khaled, M, Bille, K, Marchetti, B *et al.* (2005). Hypoxia-inducible factor 1α is a new target of microphthalmia-associated transcription factor (MITF) in melanoma cells. *J Cell Biol* **170**: 49–59.
27. Berra, E, Benizri, E, Ginouves, A, Volmat, V, Roux, D and Pouyssegur, J (2003). HIF prolyl-hydroxylase 2 is the key oxygen sensor setting low steady-state levels of HIF-1α in normoxia. *EMBO J* **22**: 4082–4090.
28. Makinen, PI, Koponen, JK, Karkkainen, AM, Malm, TM, Pulkkinen, KH, Koistinaho, J *et al.* (2006). Stable RNA interference: comparison of U6 and H1 promoters in endothelial cells and in mouse brain. *J Gene Med* **8**: 433–441.
29. Weinberg, RA and Penman, S (1968). Small molecular weight monodisperse nuclear RNA. *J Mol Biol* **38**: 289–304.
30. Natarajan, R, Salloum, FN, Fisher, BJ, Kukreja, RC and Fowler, AA 3rd (2006). Hypoxia inducible factor-1 activation by prolyl 4-hydroxylase-2 gene silencing attenuates myocardial ischemia reperfusion injury. *Circ Res* **98**: 133–140.
31. Takeda, K, Cowan, A and Fong, GH (2007). Essential role for prolyl hydroxylase domain protein 2 in oxygen homeostasis of the adult vascular system. *Circulation* **116**: 774–781.
32. Lee, RJ, Springer, ML, Blanco-Bose, WE, Shaw, R, Ursell, PC and Blau, HM (2000). VEGF gene delivery to myocardium: deleterious effects of unregulated expression. *Circulation* **102**: 898–901.
33. Trentin, D, Hall, H, Wechsler, S and Hubbell, JA (2006). Peptide-matrix-mediated gene transfer of an oxygen-insensitive hypoxia-inducible factor-1α variant for local induction of angiogenesis. *Proc Natl Acad Sci USA* **103**: 2506–2511.
34. Check, E (2005). A crucial test. *Nat Med* **11**: 243–244.
35. Bitko, V, Musiyenko, A, Shulyayeva, O and Barik, S (2005). Inhibition of respiratory viruses by nasally administered siRNA. *Nat Med* **11**: 50–55.
36. Kim, DH and Rossi, JJ (2007). Strategies for silencing human disease using RNA interference. *Nat Rev Genet* **8**: 173–184.
37. Dykxhoorn, DM and Lieberman, J (2006). Silencing viral infection. *PLoS Med* **3**: e242.
38. Raoul, C, Barker, SD and Aebischer, P (2006). Viral-based modelling and correction of neurodegenerative diseases by RNA interference. *Gene Ther* **13**: 487–495.
39. Miyata, K, Kakizawa, Y, Nishiyama, N, Harada, A, Yamasaki, Y, Koyama, H *et al.* (2004). Block catiomer polyplexes with regulated densities of charge and disulfide cross-linking directed to enhance gene expression. *J Am Chem Soc* **126**: 2355–2361.
40. Kanayama, N, Fukushima, S, Nishiyama, N, Itaka, K, Jang, WD, Miyata, K *et al.* (2006). A PEG-based biocompatible block catiomer with high buffering capacity for the construction of polyplex micelles showing efficient gene transfer toward primary cells. *ChemMedChem* **1**: 439–444.
41. Oishi, M, Nagasaki, Y, Itaka, K, Nishiyama, N and Kataoka, K (2005). Lactosylated poly(ethylene glycol)-siRNA conjugate through acid-labile β-thiopropionate linkage to construct pH-sensitive polyion complex micelles achieving enhanced gene silencing in hepatoma cells. *J Am Chem Soc* **127**: 1624–1625.
42. Kakizawa, Y, Furukawa, S, Ishii, A and Kataoka, K (2006). Organic-inorganic hybrid-nanocarrier of siRNA constructing through the self-assembly of calcium phosphate and PEG-based block aniomer. *J Control Release* **111**: 368–370.
43. Akagi, D, Oba, M, Koyama, H, Nishiyama, N, Fukushima, S, Miyata, T *et al.* (2007). Biocompatible micellar nanovectors achieve efficient gene transfer to vascular lesions without cytotoxicity and thrombus formation. *Gene Ther* **14**: 1029–1038.
44. Itaka, K, Ohba, S, Miyata, K, Kawaguchi, H, Nakamura, K, Takato, T *et al.* (2007). Bone regeneration by regulated *in vivo* gene transfer using biocompatible polyplex nanomicelles. *Mol Ther* **15**: 1655–1662.
45. Wu, S, Murai, S, Kataoka, K and Miyagishi, M (2008). Yin Yang 1 induces transcriptional activity of p73 through cooperation with E2F1. *Biochem Biophys Res Commun* **365**: 75–81.

Journal of Controlled Release 133 (2009) 198–205

Contents lists available at ScienceDirect

Journal of Controlled Release

journal homepage: www.elsevier.com/locate/jconrel

A novel strategy utilizing ultrasound for antigen delivery in dendritic cell-based cancer immunotherapy

Ryo Suzuki [a], Yusuke Oda [a], Naoki Utoguchi [a], Eisuke Namai [a], Yuichiro Taira [a], Naoki Okada [b], Norimitsu Kadowaki [c], Tetsuya Kodama [d], Katsuro Tachibana [e], Kazuo Maruyama [a,*]

[a] Department of Biopharmaceutics, School of Pharmaceutical Sciences, Teikyo University, 1091-1 Suwarashi, Sagamiko-cho, Sagamihara, Kanagawa 229-0195, Japan
[b] Department of Biotechnology and Therapeutics, Graduate School of Pharmaceutical Sciences, Osaka University, 1-6 Yamadaoka, Suita, Osaka 565-0871, Japan
[c] Department of Hematology and Oncology, Graduate School of Medicine, Kyoto University, 54 Shogoin Kawara-cho, Sakyo-ku, Kyoto 606-8507, Japan
[d] Department of Biomedical Engineering, Graduate School of Biomedical Engineering, Tohoku University, 2-1 Seiryo-machi, Aoba-ku, Sendai 980-8575, Japan
[e] Department of anatomy, School of medicine, Fukuoka University, 7-45-1 Nanakuma, Jonan-ku, Fukuoka 814-0180, Japan

ARTICLE INFO

Article history:
Received 12 August 2008
Accepted 16 October 2008
Available online 31 October 2008

Keywords:
Dendritic cells
Antigen delivery system
Cancer immunotherapy
Ultrasound
Liposomes

ABSTRACT

In dendritic cell (DC)-based cancer immunotherapy, it is important that DCs present peptides derived from tumor-associated antigens on MHC class I, and activate tumor-specific cytotoxic T lymphocytes (CTLs). However, MHC class I generally present endogenous antigens expressed in the cytosol. We therefore developed an innovative approach capable of directly delivering exogenous antigens into the cytosol of DCs; i.e., a MHC class I-presenting pathway. In this study, we investigated the effect of antigen delivery using perfluoropropane gas-entrapping liposomes (Bubble liposomes, BLs) and ultrasound (US) exposure on MHC class I presentation levels in DCs, as well as the feasibility of using this antigen delivery system in DC-based cancer immunotherapy. DCs were treated with ovalbumin (OVA) as a model antigen, BLs and US exposure. OVA was directly delivered into the cytosol but not via the endocytosis pathway, and OVA-derived peptides were presented on MHC class I. This result indicates that exogenous antigens can be recognized as endogenous antigens when delivered into the cytosol. Immunization with DCs treated with OVA, BLs and US exposure efficiently induced OVA-specific CTLs and resulted in the complete rejection of E.G7-OVA tumors. These data indicate that the combination of BLs and US exposure is a promising antigen delivery system in DC-based cancer immunotherapy.

1. Introduction

Dendritic cells (DCs), which are unique antigen-presenting cells capable of priming naive T cells, are promising vaccine carriers for cancer immunotherapy [1]. To induce efficiently a tumor-specific cytotoxic T-lymphocyte (CTL) response, DCs should abundantly present epitope peptides derived from tumor-associated antigens (TAAs) via major histocompatibility complex (MHC) class I molecules [2]. In general, the majority of peptides presented via the MHC class I molecules are generated from endogenously synthesized proteins that are degraded by the proteasome [3]. On the other hand, exogenous antigens such as TAAs for DCs are preferentially presented on MHC class II molecules [3]. In order to prime efficiently TAAs specific for CTLs, it is important to develop a novel antigen delivery system, which can induce MHC class I restricted TAA presentation on DCs. Several researchers are developing antigen delivery tools based on the cross presentation theory of exogenous antigens for DCs [4–8]. In these studies, various types of antigen delivery carriers such as liposomes [6,7], poly(γ-glutamic acid) nanoparticles [5] and cholesterol pullulan nanoparticles [8], all of which can deliver antigen into DCs via the endocytosis pathway, have been developed. We have reported that IgG modified liposomes with entrapped antigen can induce cross presentation of exogenous antigen for DCs on MHC class I molecules [9]. These carriers deliver antigens into DCs via an endocytosis mechanism, with delivery thought to be due to exogenous antigen leaking from the endosome into the cytosol. It is therefore important to design an antigen delivery system which does not rely on the endocytosis pathway. In other study, it was reported that DCs pulsed with exogenous antigens by electroporation presented their antigens on MHC class I molecules and resulted

Abbreviations: Alexa-OVA, Alexa Fluor 488-conjugated ovalbumin; BL, Bubble liposome; CTL, cytotoxic T lymphocyte; DC, dendritic cell; DSPC, 1,2-distearoyl-sn-glycero-phosphatidylcholine; DSPE-PEG(2k)-OMe, 1,2-distearoyl-sn-glycero-3-phosphatidyl-ethanolamine-methoxypolyethyleneglycol; ER, endoplasmic reticulum; FBS, fetal bovine albumin; HLA, human leukocyte antigen; MHC, major histocompatibility complex; MTT, 3-(4,5-s-dimethylthiazol-2-yl)-2,5-diphenyl tetrazolium bromide; NaN_3, sodium azide; OVA, ovalbumin; PBS, phosphate buffer saline; US, ultrasound; TAA, tumor associated antigen.

* Corresponding author. Department of Biopharmaceutics, School of Pharmaceutical Sciences, Teikyo University, 1091-1 Suwarashi, Sagamiko-cho, Sagamihara, Kanagawa 229-0195, Japan. Tel.: +81 42 685 3722; fax: +81 42 685 3432.
E-mail address: maruyama@pharm.teikyo-u.ac.jp (K. Maruyama).

0168-3659/$ – see front matter © 2008 Elsevier B.V. All rights reserved.
doi:10.1016/j.jconrel.2008.10.015